ACS OMEGA

Open Access

http://pubs.acs.org/journal/acsodf

Article

Preparation, In Vitro Characterization, and Evaluation of Polymeric pH-Responsive Hydrogels for Controlled Drug Release

Tahir Mahmood, Rai M. Sarfraz,* Asif Mahmood, Mounir M. Salem-Bekhit, Hira Ijaz, Muhammad Zaman, Muhammad R. Akram, Ehab I. Taha, Ram K. Sahu, and Yacine Benguerba

Cite This: *ACS Omega* 2024, 9, 10498−10516

Read Online

ACCESS | Metrics & More | Article Recommendations

ABSTRACT: The purpose of the current research is to formulate a smart drug delivery system for solubility enhancement and sustained release of hydrophobic drugs. Drug solubility-related challenges constitute a significant concern for formulation scientists. To address this issue, a recent study focused on developing PEG-*g*-poly(MAA) copolymeric nanogels to enhance the solubility of olmesartan, a poorly soluble drug. The researchers employed a free radical polymerization technique to formulate these nanogels. Nine formulations were formulated. The newly formulated nanogels underwent comprehensive tests, including physicochemical assessments, dissolution studies, solubility evaluations, toxicity investigations, and stability examinations. Fourier transform infrared (FTIR) investigations confirmed the successful encapsulation of olmesartan within the nanogels, while thermogravimetric analysis (TGA) and differential scanning calorimetry (DSC) studies verified their thermal stability. Scanning electron microscopy (SEM) images revealed the presence of pores on the surface of the nanogels, facilitating water penetration and promoting rapid drug release. Moreover, powder X-ray diffraction (PXRD) studies indicated that the prepared nanogels exhibited an amorphous structure. The nanogel carrier system led to a significant enhancement in olmesartan's solubility, achieving a remarkable 12.3-fold increase at pH 1.2 and 13.29-fold rise in phosphate buffer of pH 6.8 (NGP3). Significant swelling was observed at pH 6.8 compared to pH 1.2. Moreover, the formulated nexus is nontoxic and biocompatible and depicts considerable potential for delivery of drugs and protein as well as heat-sensitive active moieties.

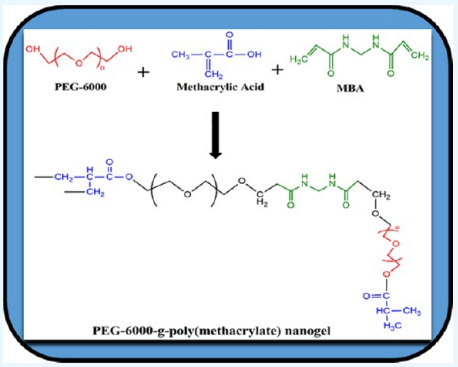

INTRODUCTION

Drug solubility has emerged as a significant concern for pharmaceutical scientists.[1] With the emergence of high-throughput screening in drug development, an increase in the number of poorly water-soluble drugs is observed. Furthermore, augmenting the bioavailability of these active moieties is a crucial challenge in drug development. Poorly soluble drugs often exhibit erratic absorption and variable bioavailability, making it challenging to achieve the desired therapeutic effects. Nanotechnology and other technologies have been employed to tackle this issue to enhance drug solubility.[2,3] One practical approach involves creating nanogels, nanosized structures formed by cross-linking hydrophilic polymers.[4] These colloidal hydrogels possess unique properties such as shape, size, charge, softness, porosity, amphiphilicity, and degradation, which can be tailored by adjusting the chemical composition of polymers.[5] To improve drug solubility, hydrogels have been pinched into a small nexus with nanosize dimensions. Furthermore, micellar architecture aids in encapsulation of hydrophobic moieties.[6] Nanogels undergo changes in response to environmental conditions and are referred to as physiologically responsive nanogels which respond to external stimuli such as pH, temperature, and ionic strength. These nanogels are also termed as hungry matrices and intelligent/smart matrix. Other biomedical applications include control implants, contact lenses, surrogate for ligaments, skin, cartilage, tendons, bones, and other dressings.[7,8] Because of their improved drug loading and great stability, nanogels are a promising drug delivery technology.[9]

Moreover, their high surface-to-volume ratio can increase the solubility of poorly water-soluble agents compared to micelles and liposomes while exhibiting better physical stability and distribution in physiological fluids.[10] Olmesartan, a drug used to treat hypertension, suffers from low bioavailability due to its poor water solubility. Oral bioavailability of olmesartan is 25.6%, which is attributed to the extensive first pass effect. It is rapidly absorbed and plasma drug concentration is achieved in

Received: October 31, 2023
Revised: January 17, 2024
Accepted: January 26, 2024
Published: February 19, 2024

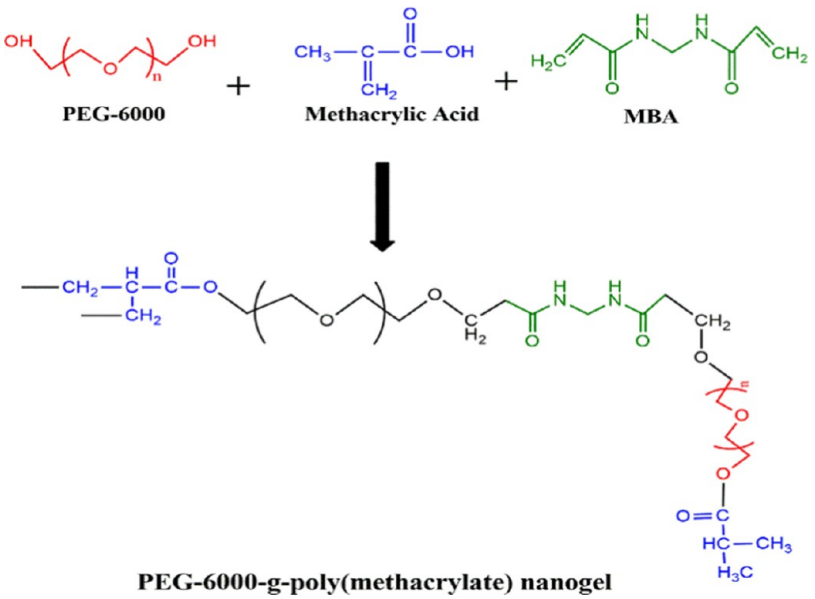

Figure 1. Proposed cross-linked diagram of PEG-*g*-poly(MAA) nanogels.

1 to 3 h.[11] To address this challenge, the study focused on developing a copolymeric nanogel carrier system using PEG-6000 through free radical polymerization.[12] The method involved grafting methacrylic acid onto PEG-6000 using methylene bis-acrylamide as a cross-linker. PEG-6000 was chosen based on a critical literature survey, and the copolymeric nanogels were characterized using swelling and release studies.[13] The PEG base hydrogel has tunable structural attributes including cross-linked density, which aids in controlled drug diffusion. Moreover, it is susceptible to changes in structural attributes without interfering in the chemistry of the network. PEG-6000, a nontoxic and water-soluble biomaterial, finds various applications in wound healing, drug delivery, and biomedical fields.[13] Earlier research has demonstrated that PEG-6000-based targeted drug delivery systems can effectively deliver peptides and proteins in a controlled manner.[13] The release of drugs from such systems is influenced by the preparation method, molecular weight, and drug solubility.[13] The incorporation of methacrylic acid (MAA) in the nanogel provides pH-responsive properties, as the carboxylic acid groups ionize into carboxylate ions in the basic environment of the gastrointestinal tract, affecting the swelling of the network.[13] *N*-Methylene bis(acrylamide) (MBA) was a cross-linker for polymerizing PEG-6000 and MAA, resulting in a more stable three-dimensional (3D) network with a gel-like architecture than that of linear chains.[14] Potassium persulfate (KPS) acted as an initiator for the polymerization of PEG-6000 and MAA.[14]

In this study, a copolymeric nanogel carrier system was formulated, which serves as a promising carrier in enhancing the solubility of poorly soluble drugs such as olmesartan. By using PEG-6000 and MAA as building blocks and MBA as a cross-linker, a stable and well-defined polymeric network with controlled swelling and drug release properties was achieved, which were evaluated by using response surface methodology. This approach may have broader applications in the development of novel drug delivery systems for other poorly soluble drugs.

MATERIALS AND METHODOLOGY

Materials. Olmesartan (active ingredient) was generously provided as a gift by Global Pharmaceuticals, Islamabad, Pakistan. Omsana 20 mg tablet (Lot number 130978, Hilton Pharma, Expiry 11/5/2021) was purchased from Servaid Pharmacy, Lahore, Punjab, Pakistan. Methylene bis-(acrylamide), methacrylic acid, and PEG 6000 were obtained from Merck, Germany. The study employed chemicals with analytical grade and freshly ready distilled water from the postgraduate lab at the College of Pharmacy, University of Sargodha, Punjab, Pakistan.

Methods. *Synthesis of PEG-g-poly(MAA) Polymeric Nanogels.* A free radical polymerization reaction was employed to cross-link the polymer (PEG-6000) and monomer (MAA) by employing a cross-linker (methylene bis(acrylamide)). The prepared solution of PEG-6000, MAA, and MBA was stirred by using a hot-plate magnetic stirrer at 37 °C and purged with nitrogen until a homogeneous mixture was obtained. The polymerization process was initiated by adding potassium persulfate continuously to the mix. Subsequently, the solution was dispensed into test tubes after sealing with aluminum foil and placed in a water bath at 70 °C for up to 24 h. After completion of the reaction, the nanogels were extracted from the test tubes and washed with a mixture of water/methanol (in 50:50 ratio) three times to eliminate any unreacted materials. The prepared nanogels were then sliced, crushed, and dried at 50 °C in a hot air oven until a constant weight of particulate was achieved. The dried particles were ground and sieved to achieve a uniform nanosized particulate system. The resulting nanogels were stored for more analysis.[14−18] The proposed chemical structure of the developed PEG-*g*-poly(MAA) nanogels is visually represented in Figure 1.

The researchers formed nine batches with varying monomer, polymer, and cross-linker contents, as outlined in Table 1. This detailed procedure illustrates the meticulous steps taken in synthesizing the PEG-*g*-poly(MAA) nanogels, ensuring reproducibility and reliability of the experimental process. The various batches prepared with different compositions also

https://doi.org/10.1021/acsomega.3c08107
ACS Omega 2024, 9, 10498−10516

Table 1. Composition of PEG-g-poly (MAA) Nanogel Formulations (NGP1-NGP9) (g/30 mL)

code	polyethylene glycol 6000	methacrylic acid	methylene bis(acrylamide)	potassium persulfate
NGP1	2	2	1	1
NGP2	4	2	1	1
NGP3	6	2	1	1
NGP4	2	4	1	1
NGP5	2	6	1	1
NGP6	2	8	1	1
NGP7	2	2	2	1
NGP8	2	2	3	1
NGP9	2	2	4	1

highlight the systematic investigation carried out to optimize the formulation and properties of the nanogels.

Drug Loading (%). The drug solution was formulated by employing a phosphate buffer of pH 6.8. The nanogels were dried, weighed, and placed in a 1% drug solution at 25 °C for loading. To secure the drug within the nanogel, the solution's pH (6.8) was controlled with a few drops of 0.1 molar HCl solution for 48 h. Subsequently, using a hot-air oven, the drug-loaded nanogels were dried at 40 °C.[13,17,19]

Characterization. *Product Yield.* The following formula was used to determine the product yield and efficiency of the process[15]

$$\text{Product yield (\%)} = \frac{M_o - M_l}{M_o} \times 100 \quad (1)$$

M_l = final weight of nanogels and M_o = collective weight of all ingredients initially.

$$\text{Product Yield} = 100 - \text{Mass loss} \quad (2)$$

Determination of the Sol–Gel Fraction. The nanogels were weighed and placed in a Soxhlet apparatus containing deionized water, which was heated to 85 °C for 12 h to determine the gel fraction. After removal from the Soxhlet apparatus with the help of a mesh screen, the nanogels were dried for 72 h at 50 °C. The gel and solution fractions were calculated using the following equation[20]

$$\text{Sol fraction (\%)} = \frac{M_i - M_e}{M_i} \times 100 \quad (3)$$

M_e and M_i represent the initial mass and mass after extraction, respectively.

$$\text{Gel fraction} = 100 - \text{Solution fraction} \quad (4)$$

Swelling Behavior. The swelling index at 37 °C was evaluated by using a 0.1 M buffer solution with pH values of 1.2 and 6.8. The nanogel particles were placed inside an empty tea bag and then submerged in the buffer solution. The tea bags and excess water were eliminated using tissue paper at predefined intervals. The weight of the swollen nanogels was determined by subtracting the weight of the empty tea bags. This entire procedure was replicated three times. The degree of swelling was subsequently calculated using the equation provided[16]

$$Q = \frac{M_s}{M_d} \quad (5)$$

M_s and M_d represent the mass of swelled particles and dried particles before immersing, respectively.

Water Absorption Study. The nanogels were weighed precisely and then immersed in distilled water at 37 °C overnight. The water absorption percentage was subsequently detected by applying the following equation

$$\%\text{Water absorption} = \frac{M_s - M_i}{M_i} \times 100 \quad (6)$$

M_s and M_i are the masses of soaked particles and dried particles before immersing, respectively.

Entrapment Efficiency (%). To assess the entrapment efficiency, a known quantity of nanogels was crushed and mixed with a buffer solution (0.1 M phosphate buffer, pH 6.8) while stirring at room temperature for 24 h. The solid residue was separated through filtration, and the remaining material was washed with a buffer solution to recover the optimal content. The resulting solution was appropriately diluted with phosphate buffer (pH 6.8) to fall within a suitable concentration range. The drug content in the solution was determined using a double-beam UV/vis spectrophotometer (UV-2600i, Shimadzu), measuring the absorbance at 257 nm and referring to a standard curve for quantification. The absorbance readings were taken in triplicate, and the average value was used for subsequent calculations. The drug loading percentage and entrapment efficiency were then calculated using the following equations as described[17]

$$\text{Drug Loading (\%)} = \frac{\text{Amount of drug in nanogel}}{\text{Amount of nanogel}} \times 100 \quad (7)$$

$$\text{Entrapment efficiency (\%)} = \frac{\text{Actual loading}}{\text{Theoretical loading}} \times 100 \quad (8)$$

Measurement of ζ-Potential and Particle Size Analysis. The average particle size of the nanogels was determined by using a particle size analyzer. For the preparation of the nanogel suspension, ultrapure water that had been filtered through a 0.22 μm filter was utilized. The particle size measurement was conducted using a zeta size analyzer from Malvern Instruments in Malvern, U.K. The dynamic light scattering (DLS) method was employed.[21,22]

Fourier Transform Infrared (FTIR) Spectroscopy. The FTIR (Fourier transform infrared) spectra of several substances, including PEG-6000, MAA (methacrylic acid), the pure drug, and the unloaded and drug-loaded nanogels, were obtained in the range of 400 to 4000 cm^{-1}. The Shimadzu FTIR-8400S was employed for this purpose. Each material was finely ground and mixed with potassium bromide (KBr) to prepare the samples for spectral recording. The resulting mixture was then analyzed using the disc slit technique.[20]

Thermal Analysis. Thermal analysis (TA) (DTG-60 simultaneous thermogravimetric and differential thermal analyzer from Shimadzu) was performed to investigate the formulated nexus's thermal stability and glass transition temperature and its substrates at elevated temperatures. This analysis involved two techniques: differential scanning calorimetry (DSC) and thermogravimetric analysis (TGA). For DSC studies, a TA Instruments (Model: DSC 2910, TA Instruments Inc., New Castle, DE) was used. A sample weighing 2 to 5 mg was carefully placed in the holder. The temperature gradually increased from 0 to 400 °C, while the

https://doi.org/10.1021/acsomega.3c08107
ACS Omega 2024, 9, 10498−10516

system was continuously purged with nitrogen gas at 20 mL/min flow rate. This process allows measuring the heat flow associated with the sample's phase transitions and thermal events. On the other hand, TGA was conducted using a Q600 TA V8.3 system. In this technique, the sample was placed in an aluminum pan, and the temperature was raised from 0 to 500 °C. TGA measures the changes in sample weight as a function of temperature, providing information about the sample's thermal stability and decomposition behavior. Both DSC and TGA are valuable tools in thermal analysis, enabling researchers to understand the thermal properties and behavior of materials under various conditions.

Scanning Electron Microscopy (SEM). For surface morphology and topological analyses of the nanogels, SEM was applied (SHIMADZU SPM-9700). In this process, the drug-loaded nanogel preparations were affixed to a metal stub by using double-sided adhesive tape and then dried within a vacuum chamber to remove any moisture. To enhance conductivity and improve imaging quality, a thin layer (around 10 nm) of gold plating was applied to the sample using a sputter coater. The nanogel samples, now coated with a conductive layer, were ready for observation under high-resolution SEM.[23−242526]

Powder X-ray Diffraction Analysis. The drug-loaded nanogels, polymers, and pure drugs underwent pXRD analysis (powder X-ray diffraction, LabX XRD-6100 SHIMADZU), and the results were compared. The X-ray diffractograms were generated by scanning the samples over 2θ values from 5 to 70 °C. By comparing the X-ray diffraction patterns of the drug-loaded nanogels, polymers, and pure drugs, we can gain insights into the crystallinity or lack thereof in each formulation.[15]

Solubility Studies. The olmesartan solubility in the prepared nanogels was detected by using a shake-flask method with pure water and buffer solutions at pH 6.8 and 1.2. The sample is added to buffer, and the suspension is shaken for a specific time period in order to formulate saturated solution. The sample is filtered, and the results were quantified using a UV/Visible spectrophotometer (UV-2600i, Shimadzu).

***In Vitro* Dissolution Studies.** The dissolution behavior of all prepared batches was assessed with a USP Type-II dissolution apparatus equipped with a paddle. Two dissolution media with different pH values, one at pH 6.8 and the other at pH 1.2, were used. Each dissolution medium had a volume of 900 mL. The dissolution process was performed at a constant temperature of 37 ± 0.2 °C, and the paddle was set to rotate at a speed of 50 rpm to ensure proper mixing. At specific intervals, 5 mL of samples was withdrawn from the vessel's center and replaced with fresh dissolution medium to maintain sink conditions. Their absorbance values were measured at 257 nm by using a UV/Visible spectrophotometer (UV-2600i, Shimadzu) to quantify the drug content in the drawn samples. This allowed for determining the amount of drug dissolved in each formulation.[27−30]

Release Kinetics. The study employed various kinetic equations (models) to analyze the drug release kinetics from the prepared nanogels. The models used included zero-order, first-order, and Highuchi, Hixson Crowell, and Korsemeyer−Peppas models. To investigate these models, the DD solver add-in in Excel was utilized. To determine the most appropriate model, the coefficient of determination (R^2 value) was used. The model with the highest R^2 value was considered the best fit for the experimental data and was used to describe the drug release behavior from the nanogels. Additionally, the value of "n" in the Korsemeyer−Peppas model was examined to understand the mechanism of drug release. When "n" was found to be 0.45, it indicated that the drug release followed Fickian diffusion, meaning that the release predominantly occurred through the diffusion of drug molecules from the nanogel matrix. If the value of "n" fell between 0.45 and 0.89, it indicated non-Fickian diffusion, implying that the release mechanism involved a combination of swelling and diffusion processes. Finally, when "n" was equal to or greater than 0.89, the drug release followed super case II transport. In this scenario, the drug was released from the nanogel constantly and sustainably over an extended period. By employing these various models and analyzing "n" in the Korsemeyer−Peppas model, researchers could gain insights into the release kinetics and mechanisms of the drug from the nanogels.[31,32]

Model-Dependent Approach. In zero-order kinetics, the drug release rate is constant over time; therefore, the amount of drug released is directly proportional to time. Therefore, the plot of drug release versus time is a straight line with a slope equal to the zero-order rate constant (K_0).

$$Q_t = Q_o - K_o t \tag{9}$$

Q_t is the amount of drug released at time t; K_0 is the zero-order rate constant; and t is time.

In first-order kinetics, the drug dissolution rate is proportional to the amount of undissolved drug present. The plot of the natural logarithm of the fraction of drug remaining versus time is a straight line with a slope equal to the negative value of the first-order rate constant (K_1).[33]

$$\ln Q_t = \ln Q_o - K_1 t \tag{10}$$

Q_t is the amount of drug dissolved at time t, Q_0 is the initial amount of drug, K_1 is the first-order rate constant, and ln is the natural logarithm.

The Korsmeyer−Peppas model is commonly used to analyze drug release from polymeric systems. The equation is as follows

$$\frac{M_t}{M_\infty} = Kt^n \tag{11}$$

where M_t/M_∞ represents the amount of drug released at time t, normalized to the total amount of drug (M_∞) in the system, K is a proportionality constant, and n is the release exponent, which describes the mechanism of drug release.

The Higuchi model is commonly used to describe drug release from a solid matrix such as a tablet or a nanoparticle. The equation is as follows

$$Q = K_H\sqrt{t} \tag{12}$$

Q is the amount of drug released at time t, K is the Higuchi dissolution constant, and t is time.

In the Higuchi model, the drug release rate is directly proportional to the square root of time, suggesting that drug release follows Fickian diffusion. This means that the drug release rate is primarily controlled by the diffusion of drug molecules through the matrix of the nanogels.[28,29]

Model-Independent Approach. Using DD solver software, the model-independent approach employs similarity ($f2$) and a difference factor ($f1$).

https://doi.org/10.1021/acsomega.3c08107
ACS Omega 2024, 9, 10498−10516

$$f2 = 50 \times \log\left\{\left[1 + \left(\frac{1}{n}\right)(R_t - T_t)^2\right]^{-0.5} \times 100\right\} \quad (13)$$

$$f1 = \left\{\frac{\left[\sum_{t=1}^{n} |R_t - T_t|\right]}{\left[\sum_{t=1}^{n} R_t\right]}\right\} \times 100 \quad (14)$$

Statistical Approach. The studies were done in triplicate, and the findings are shown as mean standard deviation (SD). The swelling ratio and medication release data were evaluated using one-way analysis of variance (ANOVA) with a significance level of $p < .05$.

Stability Studies. Stability studies of the nanogels were carried out by following the guidelines provided by the International Council for Harmonization (ICH). Accelerated stability studies were conducted for 6 months, during which the nanogels were kept at a temperature of 40 ± 2 °C and a relative humidity of 75 ± 5%. After the stability studies were completed, the nanogels were evaluated for physical characteristics, such as grittiness, syneresis, color, pH, and drug content.

***In Vitro* Biodegradation Studies.** Biodegradation studies were conducted at pH 1.2 (gastric fluid) and 6.8 (intestinal fluid) in a glass beaker. Sample-containing beakers were kept on a hot-plate magnetic stirrer at 100 rpm (stirring speed) at 37 °C. Samples were removed at a definite time interval, washed with distilled water, and subjected to lyophilization in order to calculate the dry weight. Remaining weight (%) was calculated by using the following formula

$$\text{Weight Remained (\%)} = \frac{W_d}{W_o} \times 100$$

W_d is the weight of the dried nanogel after degradation and W_o is the initial weight of the hydrogel.

Acute Toxicity Studies. According to the Organization of Economic Cooperation and Development (OECD) guidelines as well as protocols set and approved by the Institutional Research Ethics Committee, Department of Pharmacy, University of Lahore (Ethics Committee approval number IREC-2020-130), acute toxicity studies were conducted. Twelve male albino rabbits with an average weight range of 1200−2000 g were used in the study, and they were divided into two groups: a control group and a treated group. Both groups were subjected to a 12 h day/night cycle and fed a regular diet and tap water. The control group was given food and water, while the treated group was administered developed nanogels (1 g/kg). Both groups were fasted for 12 h, and any changes in physical parameters such as signs of illness, body weight, ocular toxicity, dermal toxicity, and mortality were monitored for up to 14 days. On the 14th day, sampling was performed, and hematological and biochemical analyses were conducted on both groups. The rabbits were sacrificed during histological studies, and vital organs were removed to prepare slides. A histological examination was performed using an optical microscope, and the slides from both groups were compared for a detailed histopathological examination.[12]

RESULTS AND DISCUSSION

Physical Appearance. The appearance of the prepared formulations was observed, and results were presented for the best-optimized formulation of NGP3 (Figure 2). All the nanogels prepared with PEG and methacrylic acid appeared as discrete particulate systems with a milky white appearance.

Figure 2. Physical appearance of PEG-*g*-poly(MAA) nanogels.

Product Yield. The product yield of the prepared formulations was calculated to determine the efficiency of the process. The effect of varying concentrations of individual substrates on the product yield was also evaluated. Different formulations were prepared with varying substrate concentrations, including a cross-linking agent, monomer, and polymer. Figure 3 displays the product yields of various

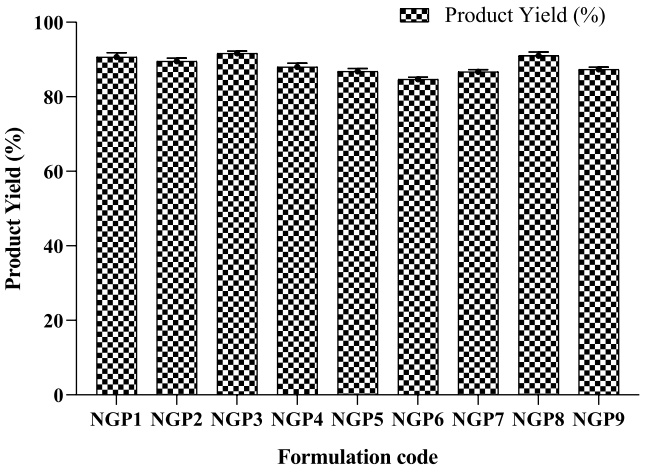

Figure 3. Product yield (%) of formulations NGP1 to NGP9.

formulations formulated with polyethylene glycol. The percentage yield (%) of nanogels ranged from 84.67 ± 0.58 to 91.67 ± 0.58%. It was observed that the product yield (%) was dependent on the concentration of PEG-600, as increasing the polymer concentration promoted the product yield. This finding is consistent with the results reported by Dhua et al. in 2022.[33]

Sol−Gel Fraction. The prepared nanogels underwent evaluation for the sol−gel fraction to determine the proportion of the unreacted polymer or monomer. The results are presented in Figure 4. Since 100% polymerization is not achievable, there are fractions of polymer and monomer that do not participate in nexus development, and these fractions constitute the sol fraction of the nanogel.[34]

https://doi.org/10.1021/acsomega.3c08107
ACS Omega 2024, 9, 10498−10516

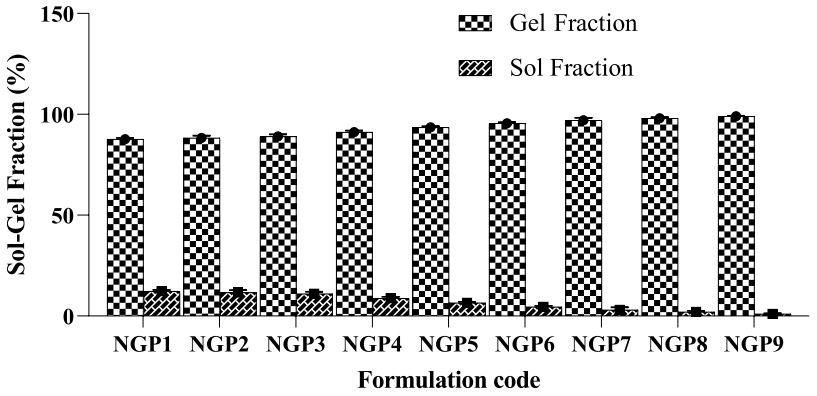

Figure 4. Sol−gel fraction evaluation of PEG-*g*-poly(MAA) nanogels.

A linear relationship was observed between the gel fraction and the polymer, monomer, or cross-linking agent concentration. Polymeric nanogels contain a significant amount of loosely attached uncross-linked polymeric macromolecules. The sol−gel fraction determines the cross-linked and uncross-linked portions of the polymeric nexus. Furthermore, a significant increase in the gel fraction was observed with incremental rises in polymer and monomer concentrations. Additionally, a higher concentration of PEG-6000 promotes a higher degree of inter- and intrahydrogen bonding, resulting in a significant increase in gel fraction, as depicted in Figure 4. Formulations NGP1 to NGP3 showed gel fractions ranging from 87.67 ± 0.58 to 89.00 ± 0.99%, with sol fractions ranging from 12.33 ± 0.58 to 11.00 ± 0.99%. Formulations NGP4 to NGP6 showed gel fractions ranging from 91.17 ± 0.76 to 95.5 ± 0.50%, with sol fractions ranging from 8.83 ± 0.76 to 4.50 ± 0.5%. Moreover, in formulations NGP7 to NGP9, the gel fraction increased with an increase in the MBA content. Formulation NGP9, which had the highest MBA content, exhibited a gel fraction of 98.99 ± 0.26%. Ijaz et al. 2019 fabricated cross-linked acrylic acid xanthan gum-based hydrogels and reported an increase in gel fraction with increasing fractions of polymers, monomers, and cross-linkers, as reported in our study.[35]

Swelling Behavior. Swelling behavior was studied in acidic (pH 1.2) and alkaline (pH 6.8) media. The uptake of swelling media increased at basic pH, while it was low at acidic pH, as shown in Figure 5. Swelling at various pH values depends on the availability of the free volume of the expanded polymeric matrix (free volume) and ionizable functional groups such as −COOH, which form an H-bond with water. At pH 6.8, carboxylic acid pK_a is about 4.5, the carboxyl group of the nanogel dissociates at pH ≥ 4.5, and osmotic pressure increases, resulting in electrostatic repulsion and pronounced swelling.[34−36] Drug release from formulated nanogels depends on swelling of the nanogel. The influence of the variable contents of PEG-6000, MAA, and MBA was evaluated. By increasing the concentration of PEG-6000, the swelling was observed from 80.83 ± 0.38 to 92.475% at pH 6.8 (Figure 5A). Swelling is directly related to the molecular weight of PEG. Moreover, electrostatic repulsion forces between the polymeric nexus and ionized carboxylic acid pendant groups aid in the swelling of the polymeric network. Mahmood et al. 2023 developed an intelligent carrier system for site specific delivery of diloxanide furoate and they have reported similar facts with respect to ionization of carboxylic groups leading to swelling of the polymeric network.[37]

The equilibrium swelling of formulations NGP4−NGP6, which contained variable amounts of MAA, increased in an upward trend from 70.44 ± 0.34 to 90.34 ± 0.34% at pH 6.8 and decreased slightly from 14.23 ± 0.34 to 13.54% at pH 1.2 (as shown in Figure 5B). A significant increase in swelling was observed at pH 6.8. At a basic pH, the −COOH groups were deprotonated. The negatively charged COO− groups caused electrostatic repulsion, resulting in the uncoiling of polymeric chains and repulsion of these chains, thus creating voids for the uptake of more swelling media. It was observed that NGP6, which contained a higher concentration of MAA, exhibited more increased swelling. Similar findings were reported by Ijaz et al. (2019), who formulated an HEC-*co*-poly(AA)-based polymeric nexus for colon targeting of perindopril erbumine.[38]

To investigate the impact of cross-linker concentration on the nanogel formulation, samples were prepared with varying concentrations of MBA and allowed to reach equilibrium at pH 6.8 and 37 °C. The results indicated that an increase in the cross-linker content led to a decrease in the uptake of swelling media. This could be attributed to a higher concentration of cross-linkers, resulting in more cross-links, reducing the pore size and free space between cross-links. Additionally, increased cross-linker concentration results in a rigid and dense network that restricts the penetration of media or macromolecular chains within the matrix, leading to a lower swelling. Equilibrium swelling was reduced from 85 to 74% as the cross-linker concentration increased (Figure 5C). Similar findings were reported by Bajpai et al. (2006) while formulating poly(methacrylamide-*co*-methacrylic acid) hydrogels.[39] Thus, previous studies have shown that increased cross-linked density decreases the mesh size, reducing equilibrium swelling.

Percentage of Water Absorption and Entrapment Efficiency (%). The nanogel particulate systems were evaluated for the water absorption percentage and entrapment efficiency. The influence of varying concentrations of cross-linking agents, polymers, and monomers on these parameters was also examined (Figure 6). The porosity of the nanogel formulation played a crucial role in governing its water absorption capacity. The entrapment efficiency of the nanogels fell within a range of 80.45−88.40%. The results indicated that with an increased PEG-6000 concentration from 2 to 6 g/30 mL, water absorbency rose from 85.45 to 92%. Similarly, when the amount of MAA was increased from 4 to 8 g/30 mL, there was a significant rise in water absorbency from 85 to 96%. However, as the MBA concentration was raised from 2 to 4 g/30 mL in the nanogels, water absorbency decreased from 83 to

https://doi.org/10.1021/acsomega.3c08107
ACS Omega 2024, 9, 10498−10516

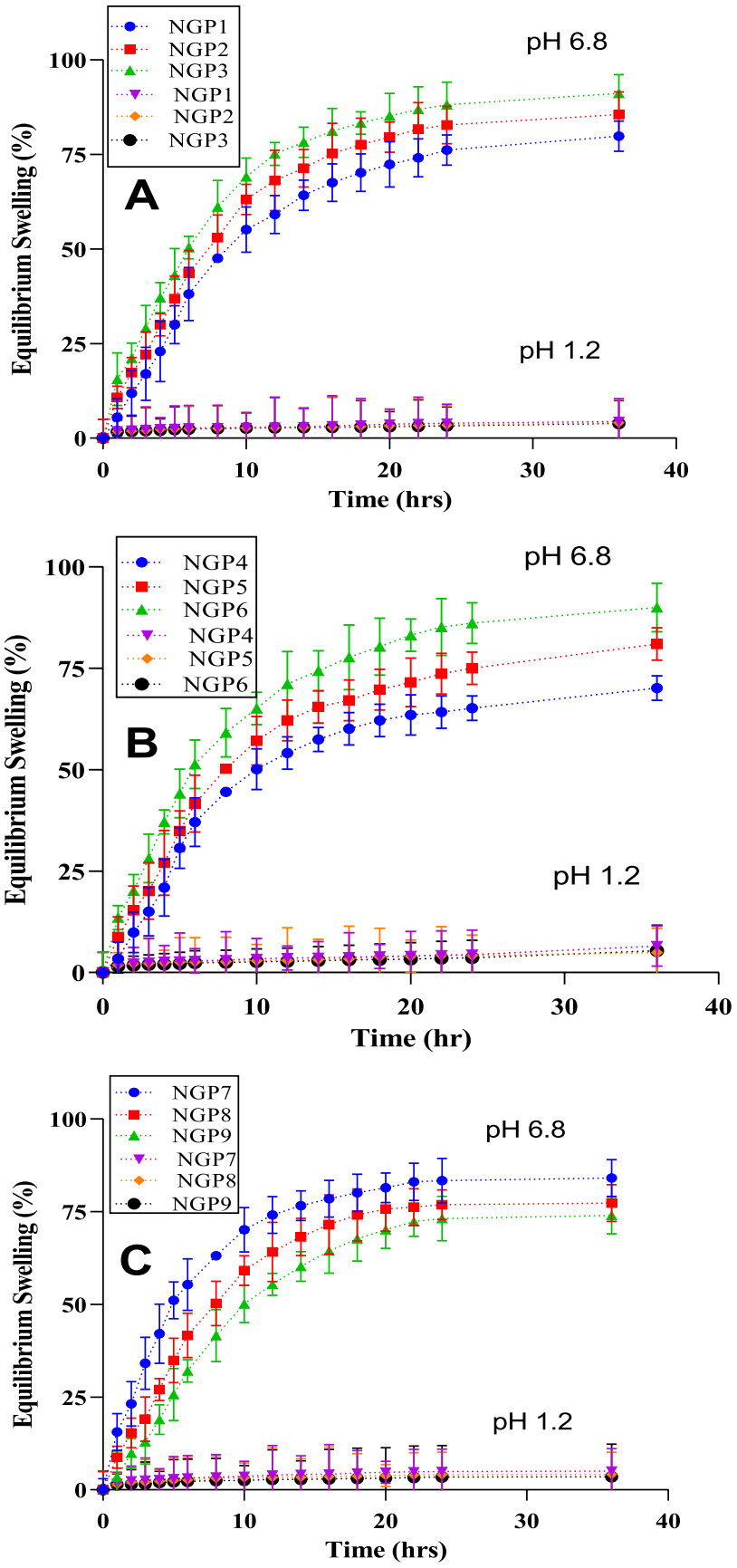

Figure 5. Influence of PEG-600 (A), MAA (B), and MBA (C) on swelling of the nanogel at pH 1.2 and 6.8.

https://doi.org/10.1021/acsomega.3c08107
ACS Omega 2024, 9, 10498−10516

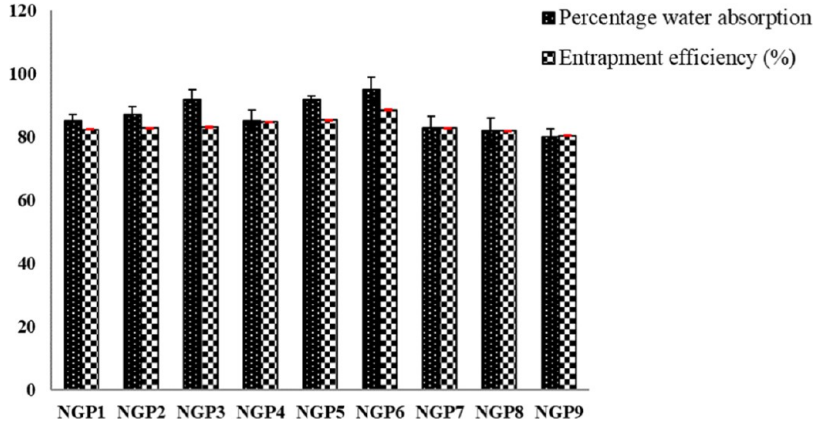

Figure 6. Effect of various ingredients on copolymerize nanogels on the percentage of water absorption and entrapment efficiency.

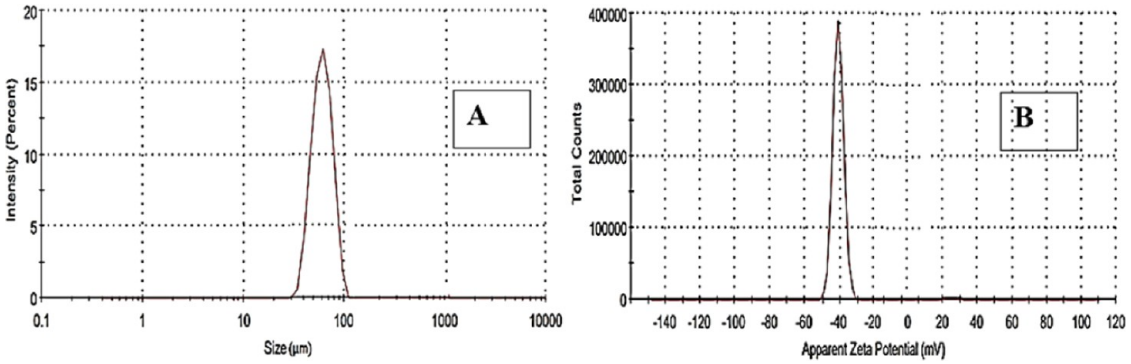

Figure 7. Average particle size (A) and ζ-potential (B) PEG-*g*-poly(MAA) copolymeric nanogels NGP3.

79.13%. These findings were consistent with a study conducted by Wen et al. in 2016, where they investigated microwave-assisted semi-interpenetrating polymeric systems.[40]

The entrapment efficiency followed a similar trend. Formulations NGP1−NGP3 exhibited entrapment efficiencies ranging from 82.45 to 83.16%, while NGP4−NGP6 showed entrapment efficiencies ranging from 64.87 to 88.55%. In contrast, formulations NGP7 to NGP9 demonstrated 82.76−80.46% entrapment efficiencies. In other words, entrapment efficiency increased with higher contents of PEG-6000 and MAA but exhibited an inverse relationship with MBA. Similar trends in entrapment efficiency were reported by Liu et al. in their study on ibuprofen-loaded amphiphilic carboxymethyl-hexanoyl chitosan-based hydrogels[41] as well as by Ijaz et al. in 2022, where they investigated the pH-responsive cross-linked CS-*co*-PAA-based nexus for targeted drug delivery.[42]

Measurement of ζ-potential and Particle Size Analysis. The average particle size distribution of the optimized NGP3 formulation was assessed, and the results are depicted in Figure 7. The particle size of the NGP3 nanogels varied within the 100−400 nm range, with the highest percentage of particles observed at 300 nm. The ζ-potential of the nanogels was found to be neutral, which suggests good stability. Furthermore, these nanogels demonstrated easy dispersibility in aqueous medium.

FTIR Spectroscopic Analysis. FTIR spectra were collected for various samples, including the pure drug, individual ingredients, the developed nanogel formulation, and the drug-loaded formulation. The purpose was to investigate the copolymeric network system's grafting pattern and complex formation. In the FTIR spectrum of PEG 6000 (Figure 8A), the characteristic peak at 1110 cm^{-1} corresponded to the ether

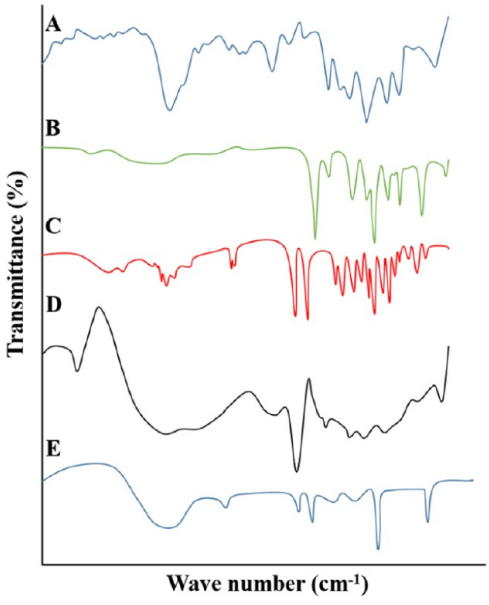

Figure 8. FTIR spectra of [A] PEG-6000, [B] MAA, [C] olmesartan, [D] unloaded PEG-*g*-poly(MAA) nanogel (NGP3), and [E] drug-loaded PEG-*g*-poly(MAA) nanogel (NGP3).

group (C−O−C) and the peak at 2880.45 cm^{-1} indicated the stretching of the alkyl groups (R-CH2). For MAA (Figure 8B), peaks at 1639, 1709, and 2973 cm^{-1} were observed, confirming the stretching of the double bond (C═C), carboxylic group (−C═O), and methyl group (−C−H), respectively. These findings were consistent with the research conducted by Ijaz et

https://doi.org/10.1021/acsomega.3c08107
ACS Omega 2024, 9, 10498−10516

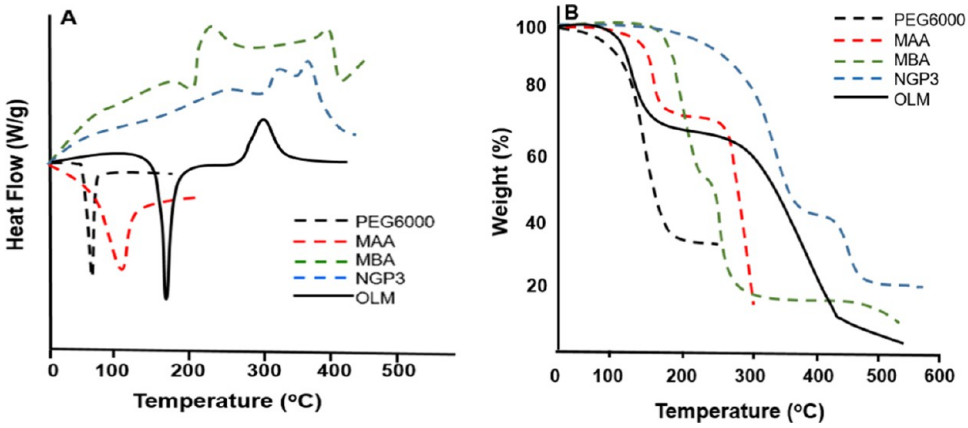

Figure 9. Thermogravimetric (TGA) (A) and DSC comparison of individual ingredients and the PEG-*g*-poly(MAA) nanogel (NGP3) (B).

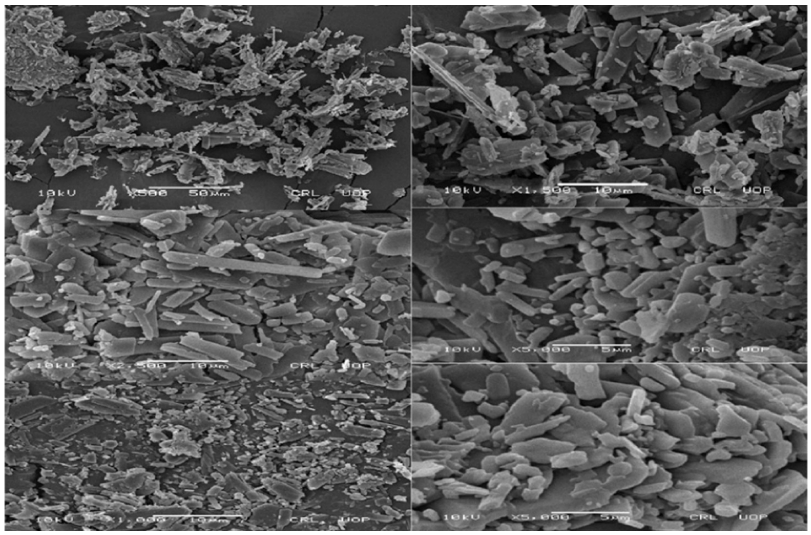

Figure 10. SEM photomicrographs of the PEG-*g*-poly(MAA) copolymeric nanogel (NGP3).

al. in 2019 on the thiolated arabinoxylan-grafted acrylic acid nexus.[43,44] The FTIR spectrum of olmesartan (Figure 8C) exhibited absorption peaks at 1033, 1571, and 1670 cm^{-1}, corresponding to the ether group (−OR), benzene ring, and carbonyl moiety (C═O), respectively. In the copolymeric nanogels of PEG-*g*-poly(MAA) (Figure 8D), a different absorption pattern was observed compared to the substrate. The absorption peak at 3200−3300 cm^{-1} disappeared and a new peak appeared in 1720−1730 cm^{-1}. This was mainly due to the addition of the C═O group from MAA and the grafting of the −OH group of PEG. A similar elimination of a distinctive peak was reported by Sarfraz et al. when creating a copolymeric network and hydrogels of *β*-CD-*g*-Poly(MAA).[14] Comparing the FTIR spectrum of the drug-loaded formulation (Figure 8E) with that of the pure drug, it was observed that the drug (olmesartan) remained intact. The significant peaks were at their original positions, i.e., 1033 and 1571 cm^{-1}, as in the pure and nanogel-entrapped drugs, as Minhas et al. reported in 2013.[36]

Thermal Analysis. The thermal stability of the individual ingredients and the formulated nanogels was assessed through thermal analysis, which involved thermogravimetric analysis (TGA) and differential scanning calorimetry (DSC). The findings of these analyses are illustrated in Figure 11. The thermal study showed that PEG exhibited an initial weight loss starting at 205 °C, leaving only 11% of its mass at 354 °C. MAA experienced rapid degradation and weight loss, with around 80% reduction at 150 °C, while MBA demonstrated a gradual weight loss (approximately 67%) from 187.6 to 344.5 °C. On the other hand, the TGA thermogram of the optimized nanogel formulation (NGP3) demonstrated excellent thermal stability, as it retained about 60% of its weight even at a high temperature of 400 °C (Figure 9B). To measure the glass transition temperature (Tg) of the prepared nanogels (NGP3) and individual ingredients, differential scanning calorimetry (DSC) was utilized (Figure 9A). Notable differences were observed in the DSC thermograms of the developed nanogel formulation and individual ingredients. Each ingredient showed specific endothermic peak patterns, MAA at 150 °C, MBA at 200 °C, and PEG-6000 at 290 °C, followed by exothermic peaks at 200, 360, and 350 °C, respectively. The shifting of these peaks toward higher temperatures indicated the successful development and grafting of the copolymeric network in the nanogel formulation. These findings are consistent with a study conducted by Anwar et al. in 2017, where they confirmed grafting by observing an exothermic peak shift at a higher temperature in creating polymeric networks using PVA and alginate.[45]

Scanning Electron Microscopy. To examine the surface morphology and topology of the prepared nanogels, SEM

https://doi.org/10.1021/acsomega.3c08107
ACS Omega 2024, 9, 10498−10516

photomicrographs of the optimized NGP3 formulation (both blank and drug-loaded) were taken at various resolutions (500 (50 μm), 500 (10 μm), 2500 (10 μm), 5000 (5 μm), 1000 (10 μm), and 5000 (5 μm)), as shown in Figure 10.

The nanogel particulate systems were seen as small irregular-shaped crystalline structures, resulting from the size reduction achieved by triturating the hydrogels.[46] The presence of white spots in the photomicrographs indicated the loading of the drug onto the nanogels. The SEM images also revealed the presence of pores on the surface of the particulate systems, which facilitated the penetration of water, buffer, and biological fluids from the surrounding media, leading to more swelling and ultimately promoting greater drug release. These findings are consistent with those of Pandav and Naik (2014), who observed improved drug release from microparticles due to water penetration through pores in the particle's surface.[47]

Powder X-ray Diffraction Analysis. In Figure 11, X-ray diffraction patterns of the pure drug, polymers, and drug-loaded nanogels are shown to analyze the crystalline or amorphous states of the drug and polymeric networks.

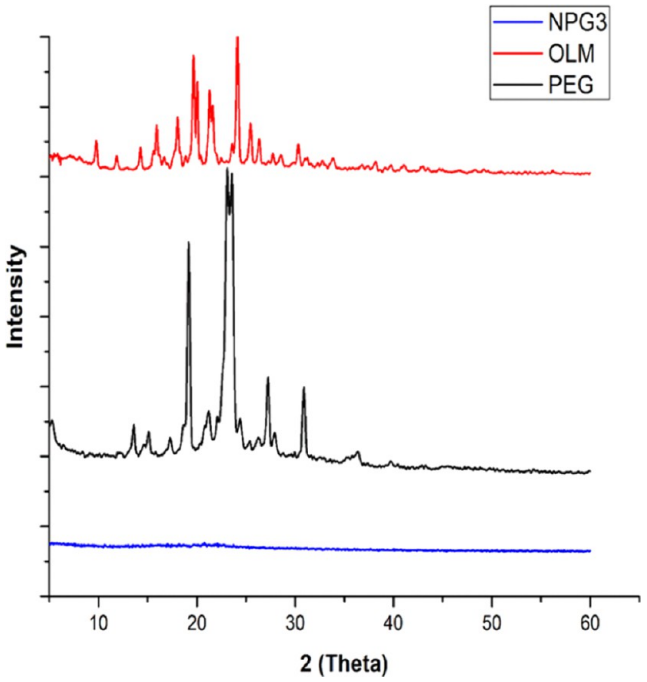

Figure 11. Comparison of XRD patterns of the polymer, drug, and drug-loaded PEG-*g*-poly(MAA) copolymeric nanogels.

The pure drug demonstrated diffraction peaks at 2θ = 11.56°, 13.04°, 20.34°, 23.45°, 29.45°, and 34.45°, confirming its crystalline nature (Figure 13). The PEG-6000 polymer exhibited distinct peaks at 2θ = 11.45°, 13.04°, 19.1°, 28.34°, and 33.34°, indicating its crystalline nature. In contrast, the prepared nanogels had no strong or sharp peaks, suggesting their amorphous nature. The amorphous nature indicates that the drug's state has become amorphous. The PXRD diffraction pattern of 5-FU-loaded nanogel disks exhibited diffuse peaks, indicating chemical interactions between the components, resulting in complex formation. The amorphous nature of the fabricated hydrogel confirmed the successful encapsulation of 5-FU within the cross-linked network, and the crystalline nature was eliminated due to cross-linking.

Solubility Studies. Due to its weak acidic nature, olmesartan becomes ionized in basic media and has a higher solubility in media with a basic pH. Solubility studies of the formulated nanogels and pure drugs were conducted in acidic and basic media. The prepared nanogels showed greater solubility in phosphate buffer with a pH of 6.8 than in HCl buffer with a pH of 1.2. However, the highest solubility of the formulated nanogels was observed in water with a neutral pH, as demonstrated in Figure 12. The solubility of the drug in the

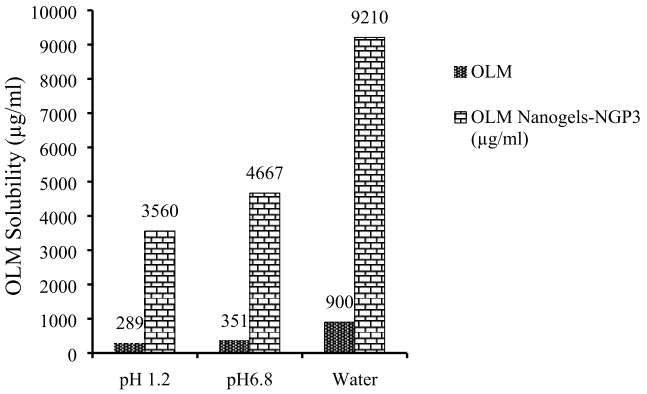

Figure 12. Graphical illustration of solubility data of the pure drug and NGP3 nanogels.

formulated nanogels was significantly increased compared with the solubility of the pure drug. For example, loading the drug into NGP3 nanogels resulted in a 10.2-fold increase in solubility in distilled water compared to pure OLM. The solubility of olmesartan nanogels was enhanced up to 12.3-fold at pH 1.2, while at pH 6.8, solubility was improved up to 13.29-fold for the NGP3 formulation.

Liu and colleagues formulated methotrexate-loaded gelatin-*co*-β-CD hydrogels and reported that complexation between the nexus significantly improved solubility and release. Additionally, complexation improved hydrophobic moieties' solubility, release, stability, and bioavailability.[48−495051525354]

Evaluation of In Vitro Drug Release. Drug release studies were performed under varying pH conditions (1.2 and 6.8) to investigate the influence of pH, cross-linking agent, monomer, and polymer contents on the drug release behavior. The findings of these drug release studies are visually presented in Figures 13 and 14, allowing for a graphical representation of the drug release patterns.

The nanogels exhibited pH-dependent drug release, with 10−12% release at pH 1.2, which increased from 79.5 to 91% at pH 6.8. The NGP3 formulation achieved a maximum drug release of 91%. This improvement in drug release at higher pH values correlated well with the swelling behavior of the nanogels, which showed better swelling at pH 6.8 compared to acidic pH. The reduced drug release at acidic pH was attributed to poor swelling, resulting in lower drug incorporation into the nanogels than that at pH 6.8. The RSM and contour plots exhibiting release data of all developed formulations (NGP1−NGP3) at pH 1.2 and 6.8 are shown in Figures 15−18. Gong et al. (2009) developed a PEG-based hydrogel and found that drug release was more significant (92.9%) in basic media than in acidic media. The increased drug release in their study was associated with a higher content of PEG-6000, which is known for its hydrophilic properties. Moradkhannejhad et al. (2020) investigated the effect of the

https://doi.org/10.1021/acsomega.3c08107
ACS Omega 2024, 9, 10498−10516

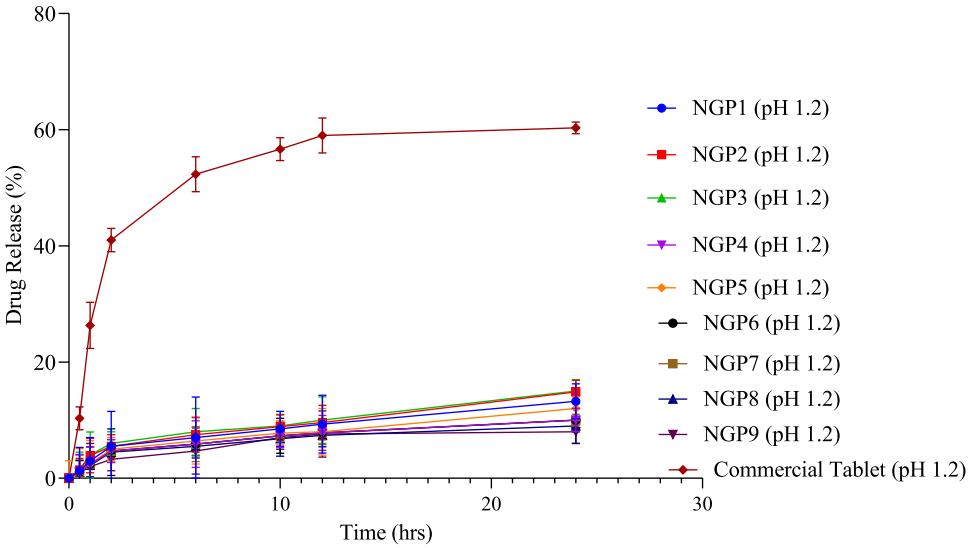

Figure 13. Influence of PEG-600, MAA, and MBA on percentage drug release from nanogels at pH 1.2.

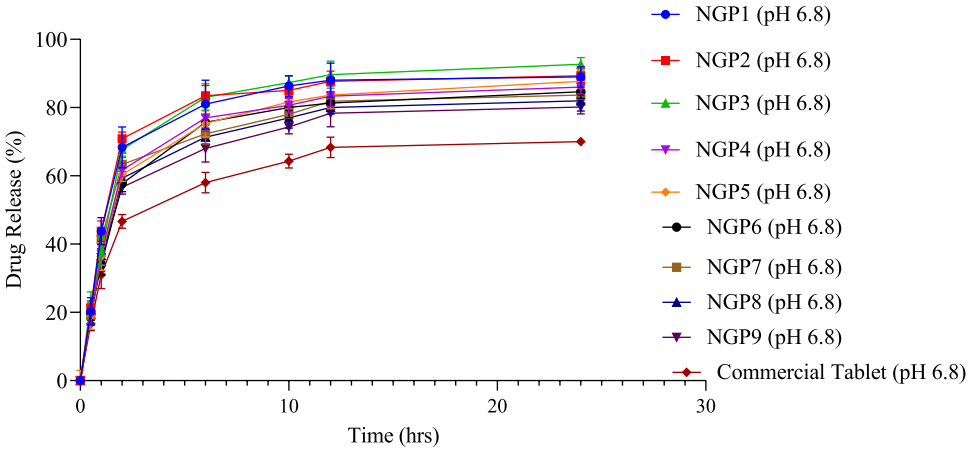

Figure 14. Influence of PEG-600, MAA, and MBA on percentage drug release from the nanogel at pH 6.8.

PEG 6000 content on drug release by creating PLA/PEG-based nanofibers. They observed that as the concentration of MAA increased from 4 to 8 g/mg in 30 mL, drug release increased from 84 to 86% at pH 6.8 and 10 to 12% at pH 1.2. This increase in drug release with a higher MAA concentration was attributed to the greater availability of −COOH pendant groups, which led to electrostatic repulsion between −COOH groups, causing polymer chain expansion.

Similarly, Ijaz et al. (2022) formulated a CS-*co*-AA-based nexus for the colon targeting of perindopril erbumine and reported similar results. As the MBA concentration increased from 2 to 4 g/mg in 30 mL, hydrogel swelling decreased from 83 to 70% at pH 6.8 and 10 to 8% at pH 1.2. The higher MBA concentration increased cross-link density, forming dense polymeric nexus and limiting water uptake into the hydrogel.

Additionally, Ijaz et al. (2019) developed a xanthan gum-based nexus for the controlled release of PE. They observed that increasing MBA concentration from 2 to 4 g/mg in 30 mL reduced hydrogel swelling from 83 to 70% at pH 6.8 and 10 to 8% at pH 1.2. This decrease in swelling was attributed to higher cross-link density, leading to a denser polymeric network that limited water uptake.

In Vitro Drug Release Kinetics. The Korsemeyer−Peppas model is widely used for evaluating drug release kinetics from polymeric matrices. It is based on the assumption that drug release occurs by combining Fickian diffusion and polymer erosion. The "*n*" value in this model indicates the drug release mechanism. If the "*n*" value is less than 0.5, it shows that drug release occurs by Fickian diffusion, whereas if it is greater than 0.5, it means non-Fickian (anomalous) diffusion. The value of "*n*" ranges between 0 and 1, with values close to 1, indicating that drug release is controlled mainly by polymer erosion.

In the present study, the "*n*" values for all developed formulations were 0.45 and 0.89, as shown in Table 2, indicating that the drug release mechanism from nanogel carrier systems followed a non-Fickian diffusion pattern. This suggests that the drug release combines diffusion and polymer erosion. The polymer matrix and the drug diffusion through the matrix influence the drug release rate. The developed nanogel carrier systems have a potential for controlled drug release due to the non-Fickian diffusion pattern, which can lead to sustained drug release over an extended period.

Stability Studies. Stability studies were conducted for 6 months on the best formulations, NGP3 and NGP6, following the ICH guidelines of accelerated temperature conditions (35 ± 5 °C) and humidity (75 ± 5%). Samples were drawn at the end of each month, and various parameters, such as the solubility study and dissolution profile, were evaluated. Results

https://doi.org/10.1021/acsomega.3c08107
ACS Omega 2024, 9, 10498−10516

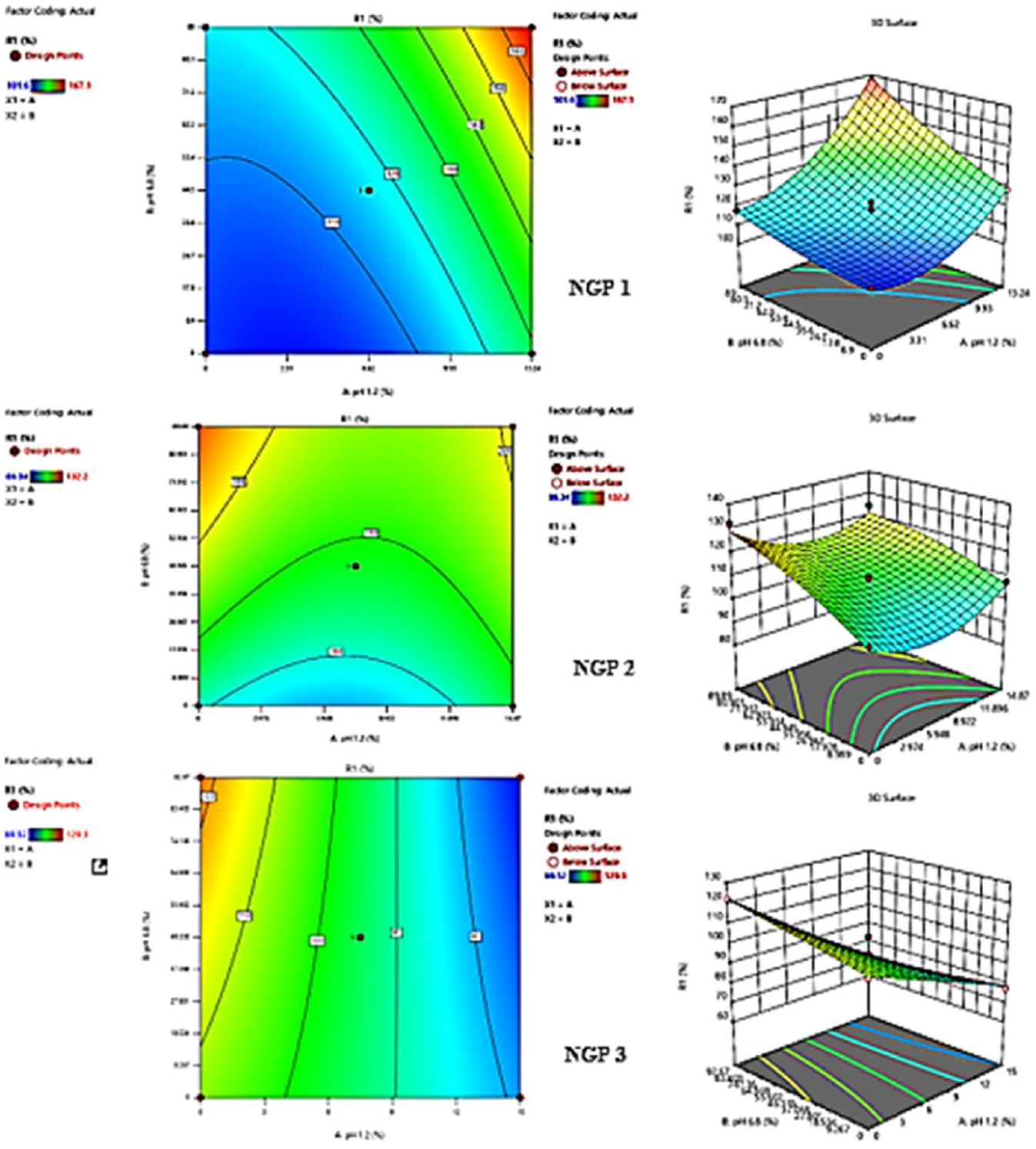

Figure 15. RSM graph and contour plots of formulations NGP1−NGP3 at pH 1.2 and 6.8.

indicated no significant change in drug contents, and the physical appearance of the stored nanogels was similar to that of the freshly prepared ones. These findings confirmed the prepared nanogels' stability under accelerated temperature and humidity conditions.

***In Vitro* Biodegradation Studies.** Biodegradation studies of the optimized formulation (NGP6) were carried out in pH 6.8. Over 12 h study, NGP6 showed 73% weight loss at pH 6.8 and 45% in pH 1.2. Mass loss was significant in both cases. Furthermore, significant degradation was observed at pH 6.8 as compared to pH 1.2 as shown in Figure 19. The nanogel remains compact and collapsed at pH 1.2, which is attributed to restricted uptake of media. Inadequate swelling is attributed to the unionized carboxylic acid group, which is due to repulsion between polymeric chains. However, at pH 6.8, carboxylic acid groups undergo ionization, which aids in the uptake of media. These findings affirm the biodegradable nature of the formulated nexus.

Acute Oral Toxicity Study of Formulated Nanogels. To confirm the biocompatibility of the newly developed

https://doi.org/10.1021/acsomega.3c08107
ACS Omega 2024, 9, 10498−10516

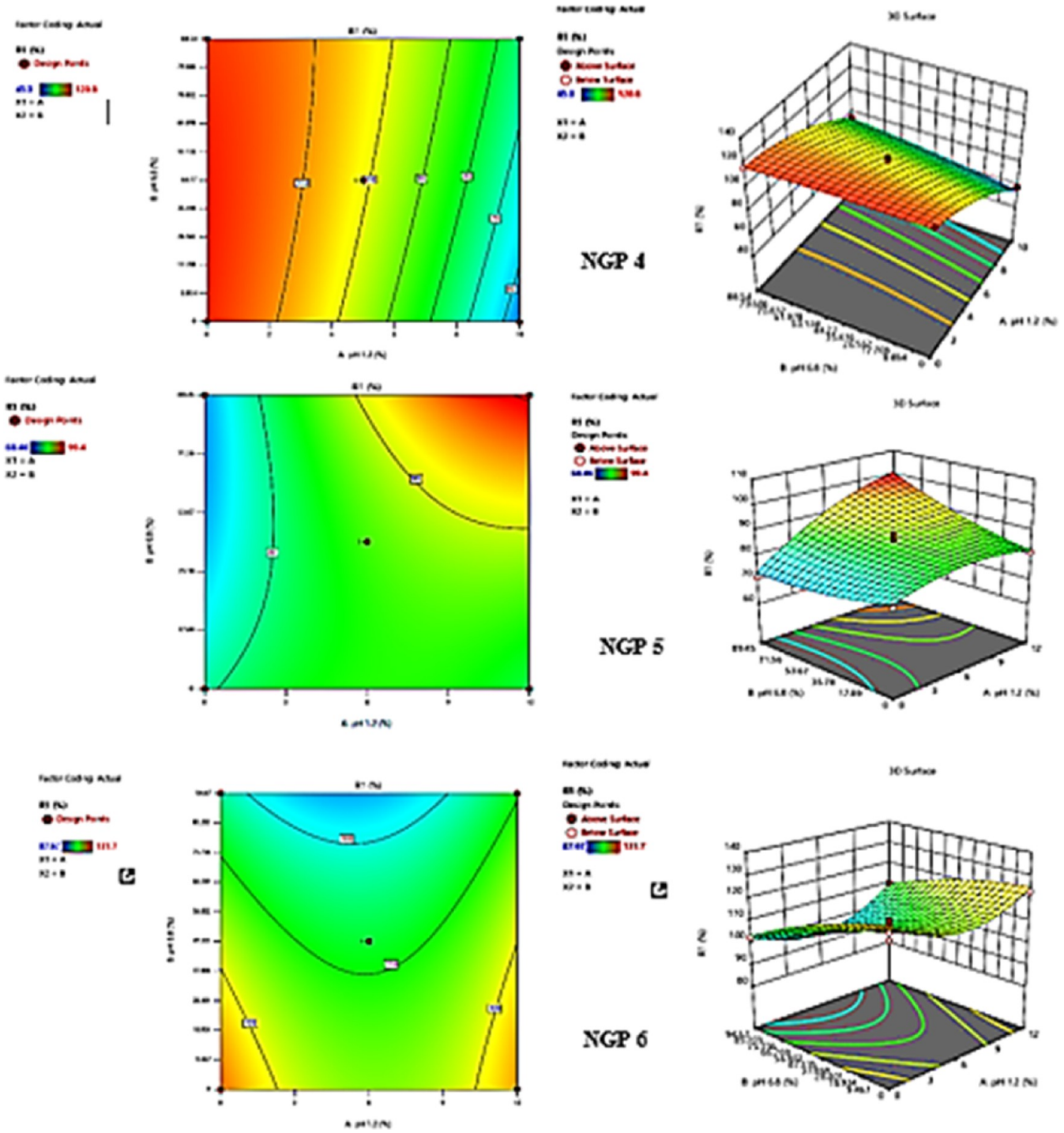

Figure 16. RSM graph and contour plots of formulation NGP4−NGP6 at pH 1.2 and 6.8.

nanogel system, an acute oral toxicological evaluation was conducted using various histopathological, biochemical, and hematological markers.[37] The testing was carried out in accordance with the Organization for Economic Cooperation and Development (OECD) criteria for chemical toxicity research. The study showed that none of the subjects exhibited any signs of morbidity and their eyes, oral cavity, hair, and skin were all in normal conditions. Moreover, their behavior activities, including breathing, reaction to stimuli, and secretions, were normal, and no edema or lacrimation was observed. Their feces were also normal without any indication of blood or pus, and their food and water intake remained normal throughout the study.

Additionally, no significant difference in body weight was reported over 14 days. The results of the acute toxicity study indicated that the formulated nanogel was safe and did not cause any motility or morbidity. More details of the study results can be found in Table 3.

Clinical Observations. All three groups of rabbits showed normal outcomes with no adverse effects on their vital organs, such as the heart, liver, kidneys, stomach, spleen, and lungs, throughout the treatment, as reported in Table 3. The oral

https://doi.org/10.1021/acsomega.3c08107
ACS Omega 2024, 9, 10498−10516

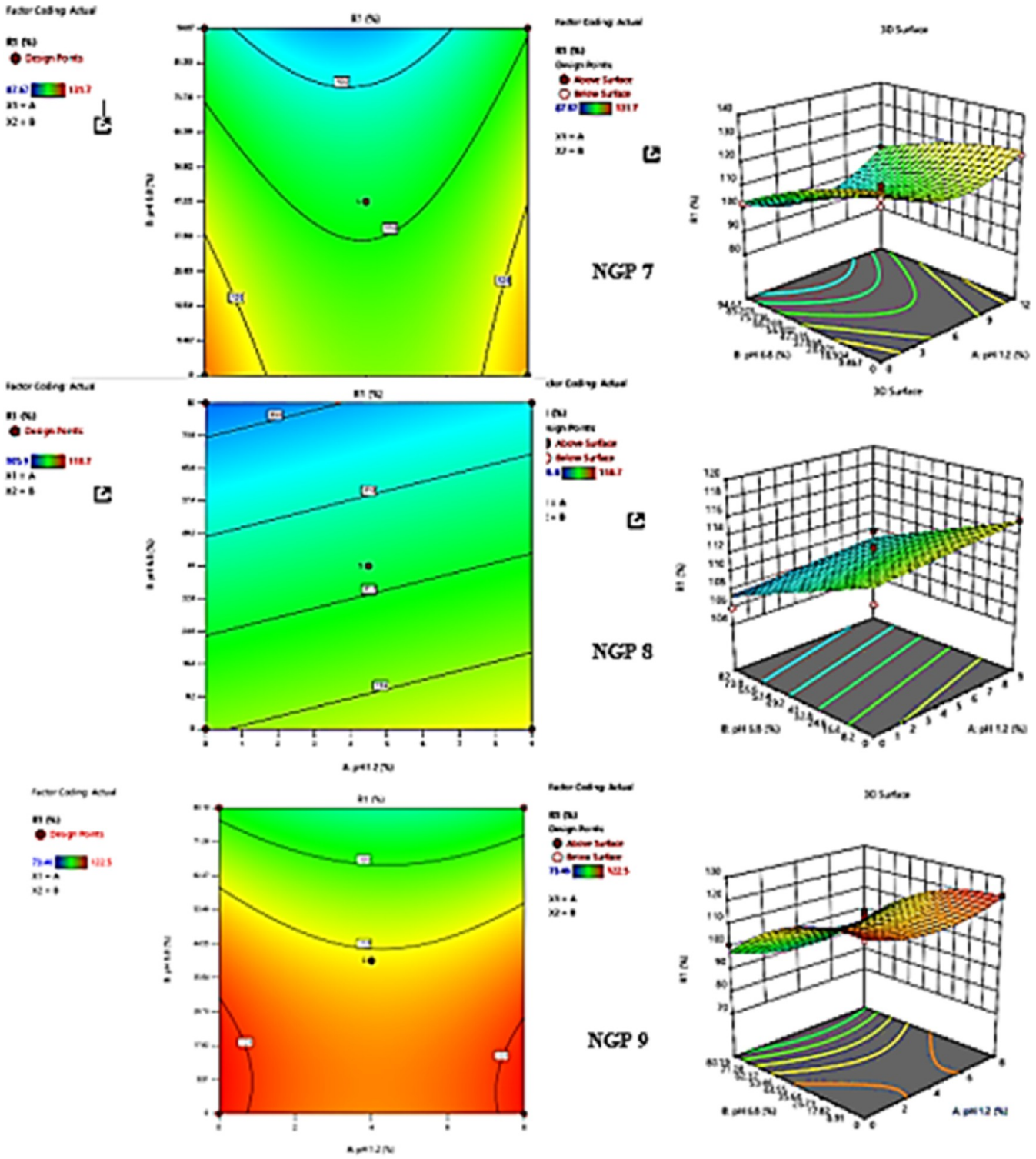

Figure 17. RSM graph and contour plots of formulations NGP7−NGP9 at pH 1.2 and 6.8.

administration of nanogels did not affect body weight or nutritional intake or cause any toxin-related issues. The rabbits exhibited no signs of skin discomfort or other behavioral changes, and their food and water intakes remained consistent throughout the trial. The amount of nutrients consumed is an essential parameter for determining the level of toxicity. These findings confirmed the clinical safety of the developed nanogel formulations. No symptoms of illness, such as a runny nose, watery eyes, saliva, or vomiting, were observed after nanogel administration. According to the globally harmonized standard (GHS), if the LD_{50} value of a testing chemical exceeds 2000 mg/kg dosage, it is categorized as "Category 5" with a toxicity score of "zero".[55] Based on this standard, the developed nanogel formulations can be classified as Category 5 with a zero-toxicity score.

Hematological Analysis. Blood samples were collected from rabbits and analyzed by using a hematology analyzer to assess the potential hematological effects of the developed

https://doi.org/10.1021/acsomega.3c08107
ACS Omega 2024, 9, 10498−10516

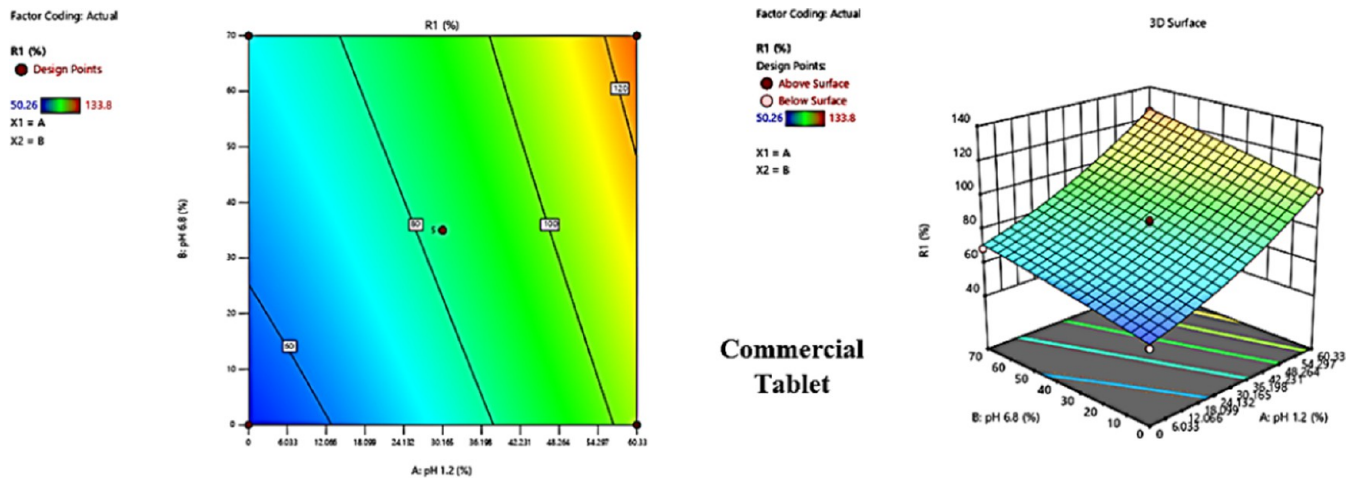

Figure 18. RSM graph and contour plots of commercial tablets at pH 1.2 and 6.8.

formulation. The results of the biochemical examination are presented in Table 4 and include various parameters such as hemoglobin (Hb) levels, platelet count, white blood cell count (WBC), red blood cell count (RBC), mean corpuscular volume (MCV), mean corpuscular hemoglobin (MCH), and mean corpuscular hemoglobin concentration (MCHC).

The Hb levels were 13.6 ± 0.9 and 15.2 ± 0.9 g/dL for the control and treated groups, respectively. The pH levels in both groups were 7.4 ± 0.9. The WBC counts were 7.1 ± 1.5 and 7.1 ± 0.25 × 109/L for the control and treated groups, respectively. The RBC count was 6.4 ± 0.9 × 10^6/mm^3 in both groups. The platelet count was 4.12 ± 1.0 10^9/L in the control group and 4.2 ± 0.90 × 10^9/L in the treated group. The monocyte count was 3.2 ± 1.1 and 3.0 ± 0.60% in the control and treated groups, respectively. The lymphocyte counts were 69 ± 1.0 and 71 ± 1.00% in the control and treated groups, respectively. The MCH values were 21.9 ± 1.00 and 22.80 ± 0.90 pg/cell for the control and treated groups, respectively, as shown in Table 4. These results indicate no significant differences in the blood parameters between the control and treated groups, suggesting that the developed formulation did not cause hematological toxicity.

Biochemical Blood Analysis. Table 5 displays the results of the biochemical analysis. The control and treated groups showed comparable values for various parameters, indicating no significant differences between them. For ALT (alanine aminotransferase) levels, the control group had 169 IU/L, while the treated group had 172 IU/L. Similarly, for AST (aspartate aminotransferase) levels, the control group showed 77 IU/L and the treated group showed 78 IU/L. Creatinine levels in the control and treated groups were 1.29 and 1.28 mg/dL, respectively.

Additionally, the urea levels were 13.9 mmol/L in the control group and 14.2 mmol/L in the treated group. The control group had 3.1 mg/dL for uric acid levels, while the treated group had 3.2 mg/dL. Moreover, the cholesterol levels were 80 mg/dL in the control group and 76 mg/dL in the treated group. Lastly, the triglyceride levels were 1.49 mmol/L in the control group and 1.52 mmol/L in the treated group. Importantly, all these biochemical parameters fell within normal ranges for the control and treated groups, suggesting that the formulated nanogel was safe and nontoxic, as it did not cause adverse effects on these parameters.

Histopathological Study. The microscopic examination of the vital organs showed no signs of histopathological lesions, indicating that the formulated nanogels did not cause any damage to the organs of the rabbits. Figure 20 shows no significant difference in organ weight between the control and treated groups, indicating that the formulated nanogels had no adverse effects on organ weight. Figure 21 shows the histological views of various organs of rabbits in the control and treated groups, which also confirm that there were no histopathological lesions in the treated group.

The maximum tolerated dose of the prepared formulations was estimated to be >10 g/kg in rabbits. This indicates that the rabbits could tolerate a high amount of the formulated nanogels without any adverse effects. Microscopic images of the spleen and brain were normal in both the control and treated groups, indicating that the formulated nanogels did not cause any damage to these organs. The lungs showed no signs of ulceration, inflammation, or infiltration, and the alveoli, bronchioles, and bronchus were normal. The glomerulus of the kidneys was also normal and showed no signs of degeneration. The stomach mucosa and muscular layer were also intact, confirming the formulated nanogels' safety.

Overall, the microscopic examination of vital organs, organ weight analysis, and histological views of various organs in both the control and treated groups indicate that the formulated nanogels were nontoxic, safe, and biocompatible. These findings suggest that the formulated nanogels could be a potential strategy to enhance drug solubility and stability.

■ CONCLUSIONS

This study focuses on creating amorphous nanogels by chemically cross-linking PEG 6000 with methacrylic acid. These nanogels serve as carriers to enhance the solubility of olmesartan, which is classified as a BCS Class-II drug. Only limitation of the hydrogel formulation is optimal selection of the formulation parameter for optimizing the drug loading as well as release. The PXRD study confirmed the amorphous nature of these nanogels, leading to improved drug bioavailability and reduced irritant effects on the gastrointestinal mucosal membrane. Various physicochemical properties (TGA, DSC, PXRD, and FT-IR) were investigated, demonstrating favorable interactions between olmesartan and the nanogel carrier system. This interaction facilitated a significant improvement in the solubility of olmesartan, up to

https://doi.org/10.1021/acsomega.3c08107
ACS Omega 2024, 9, 10498−10516

Table 2. Drug Release Kinetics (*In Vitro*) of Nanogels Comprising PEG-g-poly(MAA) Nanogel Preparations Having varying PEG Concentration

model	parameters	NGP1		NGP2		NGP3		NGP4		NGP5		NGP6		NGP7		NGP8		NGP9	
		pH 1.2	pH 6.8	pH 1.2	pH 6.8	pH 1.2	pH 6.8	pH 1.2	pH 6.8	pH 1.2	pH 6.8	pH 1.2	pH 6.8	pH 1.2	pH 6.8	pH 1.2	pH 6.8	pH 1.2	pH 6.8
zero order	K_o	4.26	35.13	4.40	36.09	4.54	36.2	4.20	33.71	4.01	33.64	3.91	32.65	4.01	32.81	3.94	31.62	3.81	30.464
	R^2	0.63	0.89	0.55	0.86	0.44	0.88	0.64	0.90	0.66	0.92	0.70	0.92	0.64	0.88	0.69	0.91	0.68	0.9252
first order	K_1	0.04	0.69	0.04	0.75	0.04	0.74	0.04	0.64	0.04	0.63	0.04	0.59	0.04	0.61	0.04	0.56	0.04	0.529
	R^2	0.99	0.97	0.99	0.97	0.49	0.98	0.68	0.98	0.69	0.98	0.73	0.98	0.67	0.99	0.72	0.98	0.71	0.9850
Higuchi	K_H	6.47	52.00	6.72	53.64	6.97	53.69	6.38	49.8	6.09	49.57	5.92	48.14	6.08	48.6	5.96	46.65	5.77	44.922
	R^2	0.97	0.93	0.95	0.93	0.91	0.93	0.97	0.93	0.97	0.92	0.97	0.93	0.97	0.94	0.98	0.933	0.97	0.9393
Korsemeyer–Peppas	K_{Kp}	7.01	46.22	7.52	49.27	8.08	48.11	6.90	43.55	6.52	42.4	6.21	41.41	6.59	43.93	6.34	40.40	6.13	38.761
	R^2	0.98	0.95	0.99	0.95	0.99	0.95	0.99	0.963	0.98	0.96	0.98	0.96	0.98	0.96	0.99	0.96	0.98	0.9726
	n	0.38	0.66	0.33	0.62	0.27	0.65	0.38	0.69	0.39	0.72	0.43	0.71	0.38	0.64	0.41	0.70	0.41	0.708

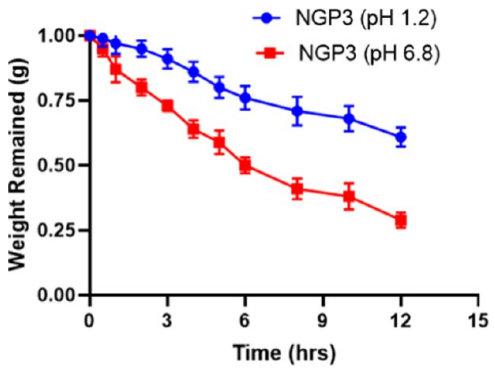

Figure 19. Biodegradation studies of the optimized formulation (NGP3) at pH 1.2 and pH 6.8.

Table 3. Clinical Findings from Acute Oral Toxicity Tests for Various Formulations

findings	group I (control)	group II (treated with NGP3 nanogels) 10 g/kg/b.w
illness symptoms	nil	nil
body weight (kg)		
pretreatment	2.10 ± 0.5	2.11 ± 1.0
day 1	2.11 ± 1.3	2.12 ± 0.9
day 7	2.15 ± 1.1	2.12 ± 0.9
day 14	2.12 ± 0.9	1.99 ± 0,6
water intake (mL)		
pretreatment	200.00 ± 1.0	200 ± 1.0
day 1	201 ± 0.9	202 ± 0.9
day 7	198 ± 0.6	199 ± 0.5
day 14	208 ± 0.6	200 ± 0.6
food intake (g)		
pretreatment	72 ± 1.0	74 ± 1.0
day 1	74 ± 0.9	73 ± 0.6
day 7	70 ± 0.8	76 ± 0.8
day 14	69 ± 1.0	72 ± 0.9
dermal toxicity:	no	no
dermal irritation		
ocular toxicity:	no	no
simple irritation or corrosion		
mortality	no	no

Table 4. Rabbits' Biochemical Blood Analysis

hematology	group I (control)	group II (treated with NGP 3 nanogels) 1–10 g/kg
Hb g/dL	13.6 ± 0.9	15.2 ± 0.9
pH	7.4 ± 0.9	7.4 ± 0.9
WBCs × 10^9/L	7.1 ± 1.5	7.1 ± 0.25
RBCs × 10^6/mm^3	6.4 ± 0.9	6.4 ± 0.9
platelets × 10^9/L	4.12 ± 1.0	4.2 ± 0.90
monocytes%	3.2 ± 1.1	3.0 ± 0.60
neutrophils%	52 ± 1.00	52 ± 0.9
lymphocytes%	69 ± 1.0	71 ± 1.00
MCV %	64 ± 1.0	61.0 ± 0.9
MCH pg/cell	21.9 ± 1.00	22.80 ± 0.90
MCHC %	30 ± 1.00	30.8 ± 1.00

13.29 times, particularly in the optimized formulation NGP6. The optimized formulation NGP6 containing 8 g/mg MAA showed 86% drug release in pH 6.8 and 12% in pH 1.2. Safety and biocompatibility of the formulated nanogels were assessed

https://doi.org/10.1021/acsomega.3c08107
ACS Omega 2024, 9, 10498−10516

Table 5. Liver, Kidney, and Lipid Profiles of Rabbits Treated with Prepared Formulations

biochemical analysis	group-I (control)	group II (treated nanogels, NGP3) 1−10 g/kg
ALT (IU/L)	169 ± 0.34	172 ± 0.66
AST (IU/L)	77 ± 0.34	78 ± 0.56
creatinine (mg/dL)	1.29 ± 0.56	1.28 ± 0.56
urea (mmol/L)	13.9 ± 0.45	14.2 ± 0.65
uric acid (mg/dL)	03.1 ± 0.56	03.2 ± 0.56
cholesterol (mg/dL)	80 ± 0.86	76 ± 0.56
triglyceride (mmol/L)	1.49 ± 0.56	1.52 ± 0.34

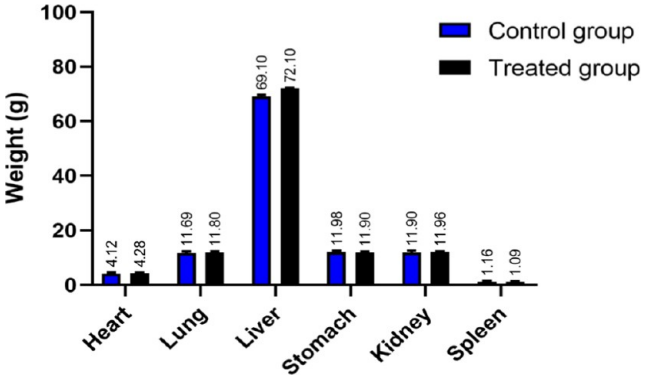

Figure 20. Organ weight from the control and treated groups during toxicity studies.

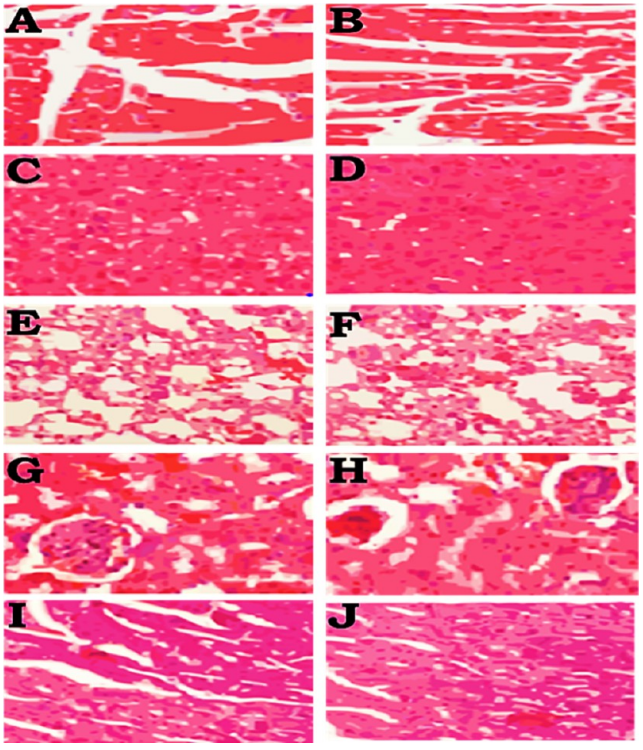

Figure 21. Histological view of a rabbit's various organs such as the spleen (control (A) and treated (B)), brain (control (C) and treated (D)), lungs (control (E) and treated (F)), kidney (control (G) and treated (H)), and intestine (control (I) and treated (J)) at 40× magnification power.

through acute oral toxicity studies conducted in healthy rabbits. The toxicology data derived from hematological, biochemical, and histological analyses showed no toxic effects, indicating that the nanogels were well-tolerated and did not cause adverse reactions in the animal body. These findings further support the potential of these amorphous nanogels as promising carrier systems for enhancing the solubility and bioavailability of olmesartan.

AUTHOR INFORMATION

Corresponding Author

Rai M. Sarfraz − *College of Pharmacy, University of Sargodha, Sargodha 40100, Pakistan*; Phone: +923338976189; Email: Sarfrazrai85@yahoo.com

Authors

Tahir Mahmood − *College of Pharmacy, University of Sargodha, Sargodha 40100, Pakistan*

Asif Mahmood − *Department of Pharmacy, University of Chakwal, Chakwal 48800, Pakistan*

Mounir M. Salem-Bekhit − *Department of Pharmaceutics, College of Pharmacy, King Saud University, Riyadh 11451, Saudi Arabia*

Hira Ijaz − *Department of Pharmaceutical Sciences, Pak-Austria Fachhochschule Institute of Applied Sciences and Technology, Haripur 22620, Pakistan*

Muhammad Zaman − *Faculty of Pharmacy, University of Central Punjab, Lahore 54000, Pakistan*; orcid.org/0000-0003-1768-2979

Muhammad R. Akram − *College of Pharmacy, University of Sargodha, Sargodha 40100, Pakistan*

Ehab I. Taha − *Department of Pharmaceutics, College of Pharmacy, King Saud University, Riyadh 11451, Saudi Arabia*

Ram K. Sahu − *Department of Pharmaceutical Sciences, Hemvati Nandan Bahuguna Garhwal University (A Central University), Tehri Garhwal 249161, India*; orcid.org/0000-0001-5671-6591

Yacine Benguerba − *Laboratoire de Biopharmacie Et Pharmacotechnie (LPBT), Ferhat Abbas Setif 1 University, Setif 19000, Algeria*; orcid.org/0000-0002-8251-9724

Complete contact information is available at: https://pubs.acs.org/10.1021/acsomega.3c08107

Notes

The authors declare no competing financial interest.

ACKNOWLEDGMENTS

The authors would like to extend their sincere appreciation to the Researchers Supporting Project Number (RSPD2024R986), King Saud University, Riyadh, Saudi Arabia.

REFERENCES

(1) Rupvate, S. R.; Gangurde, S. A.; Adavadkar, P. R.; Ukhade, S. S.; Lale, S. S. Solid self-emulsifying pellets: Solubility enhancement for oral delivery of poorly soluble BCS Class II drug. *J. Drug Delivery Ther.* **2022**, *12*, 171−176.

(2) Park, H.; Otte, A.; Park, K. Evolution of drug delivery systems: From 1950 to 2020 and beyond. *J. Controlled Release* **2022**, *342*, 53−65.

(3) Ramburrun, P.; Khan, R. A.; Choonara, Y. E. Design, preparation, and functionalization of nanobiomaterials for enhanced

https://doi.org/10.1021/acsomega.3c08107
ACS Omega 2024, 9, 10498−10516

efficacy in current and future biomedical applications. *Nanotechnol. Rev.* **2022**, *11*, 1802−1826.
(4) Ahmad, A.; Ahmad, M.; Minhas, M. U.; Sarfraz, M.; Sohail, M.; Khan, K. U.; Tanveer, S.; Ijaz, S. Synthesis and Evaluation of Finasteride-Loaded HPMC-Based Nanogels for Transdermal Delivery: A Versatile Nanoscopic Platform. *BioMed Res. Int.* **2024**, *2024*, No. 9846926.
(5) Soni, K. S.; Desale, S. S.; Bronich, T. K. Nanogels: An overview of properties, biomedical applications and obstacles to clinical translation. *J. Controlled Release* **2016**, *240*, 109−126.
(6) Soni, G.; Yadav, K. S. Nanogels as potential nanomedicine carrier for treatment of cancer: A mini review of the state of the art. *Saudi Pharm. J.* **2016**, *24*, 133−139.
(7) Oh, J. K.; Drumright, R.; Siegwart, D. J.; Matyjaszewski, K. The development of microgels/nanogels for drug delivery applications. *Prog. Polym. Sci.* **2008**, *33*, 448−477.
(8) Hamidi, M.; Azadi, A.; Rafiei, P. Hydrogel nanoparticles in drug delivery. *Adv. Drug Delivery Rev.* **2008**, *60*, 1638−1649.
(9) Mongia, P.; Khatik, R.; Raj, R.; Jain, N.; Pathak, A. K. PH-sensitive eudragit S-100 coated chitosan nanoparticles of 5-amino salicylic acid for colon delivery. *J. Biomater. Tissue Eng.* **2014**, *4*, 738−743.
(10) Zhang, H.; Zhai, Y.; Wang, J.; Zhai, G. New progress and prospects: The application of nanogel in drug delivery. *Mater. Sci. Eng., C* **2016**, *60*, 560−568.
(11) Scott, L. J.; McCormack, P. L. Olmesartan Medoxomil. *Drugs* **2008**, *68*, 1239−1272.
(12) Matsuoka, S. I.; Kikuno, T.; Takagi, K.; Suzuki, M. Poly (ethylene glycol)-induced acceleration of free radical polymerization of methyl methacrylate: Effects of highly viscous solvent and kinetic study. *Polym. J.* **2010**, *42* (5), 368−374.
(13) Sarfraz, R. M.; Akram, M. R.; Ali, M. R.; Mahmood, A.; Khan, M. U.; Ahmad, H.; Qaisar, M. N. Development and In-Vitro Evaluation of pH Responsive Polymeric Nano Hydrogel Carrier System for Gastro-Protective Delivery of Naproxen Sodium. *Adv. Polym. Technol.* **2019**, *2019*, No. 6090965, DOI: 10.1155/2019/6090965.
(14) Sarfraz, R. M.; Ahmad, M.; Mahmood, A.; Akram, M. R.; Abrar, A. Development of β-cyclodextrin-based hydrogel microparticles for solubility enhancement of rosuvastatin: an in vitro and in vivo evaluation. *Drug Des. Dev. Ther.* **2017**, *11*, 3083.
(15) Sani Mamman, I.; Teo, Y. Y.; Misran, M. Synthesis, characterization and rheological study of Arabic gum-grafted-poly (methacrylic acid) hydrogels. *Polym. Bull.* **2021**, *78*, 3399−3423.
(16) Wang, X.; Cheng, D.; Liu, L.; Li, X. Development of poly (hydroxyethyl methacrylate) nanogel for effective oral insulin delivery. *Pharm. Dev. Technol.* **2018**, *23*, 351−357.
(17) Khan, K. U.; Minhas, M. U.; Sohail, M.; Badshah, S. F.; Abdullah, O.; Khan, S.; Munir, A.; Suhail, M. Synthesis of PEG-4000-co-poly (AMPS) nanogels by crosslinking polymerization as highly responsive networks for enhancement in meloxicam solubility. *Drug Dev. Ind. Pharm.* **2021**, *47*, 465−476.
(18) Badshah, D.; Faisal, S.; Khan, D.; Ullah, K.; Malik, D.; Shamshad, N.; Suhail, D.; Jan, D. Structural and In-Vitro Characterization of Highly Swellable β-Cyclodextrin Polymeric Nanogels Fabricated by Free Radical Polymerization for Solubility Enhancement of Rosuvastatin. *Particulate Sci. Technol.* **2023**, *41* (8), 1131−1145.
(19) Mackiewicz, M.; Stojek, Z.; Karbarz, M. Synthesis of crosslinked poly (acrylic acid) nanogels in an aqueous environment using precipitation polymerization: unusually high volume change. *R. Soc. Open Sci.* **2019**, *6*, No. 190981.
(20) Mohammadi, M.; Arabi, L.; Alibolandi, M. Doxorubicin-loaded composite nanogels for cancer treatment. *J. Controlled Release* **2020**, *328*, 171−191.
(21) Hassan, Z. U.; Bashir, S.; Sarfraz, R. M.; Haroon, B.; Farid, B.; Mahmood, T. Comparative Effectiveness of β-Cyclodextrin Based Co-polymeric Hydrogel Matrices for Solubility and Bioavailability Enhancement of Lovastatin: In Vitro-In Vivo Evaluation. *Lat. Am. J. Pharm.* **2021**, *40*, 822−833.
(22) Mahmood, T.; Sarfraz, R. M.; Akram, M. R.; Ismail, A.; Qaisar, M. N.; Shah, P. A. Synthesis of CS-g-poly (MAA) Nanogels Carrier System to Improve the Solubility of Olmesartan Medoxomil and its In Vitro Evaluation. *Lat. Am. J. Pharm.* **2021**, *40*, 978−990.
(23) Rey, M.; Fernandez-Rodriguez, M. A.; Karg, M.; Isa, L.; Vogel, N. Poly-N-isopropylacrylamide nanogels and microgels at fluid interfaces. *Acc. Chem. Res.* **2020**, *53*, 414−424.
(24) Nakamura, K.; Murray, R. J.; Joseph, J. I.; Peppas, N. A.; Morishita, M.; Lowman, A. M. Oral insulin delivery using P (MAA-g-EG) hydrogels: effects of network morphology on insulin delivery characteristics. *J. Controlled Release* **2004**, *95*, 589−599.
(25) Sarfraz, R.; Khan, H.; Mahmood, A.; Ahmad, M.; Maheen, S.; Sher, M. Formulation and evaluation of mouth disintegrating tablets of atenolol and atorvastatin. *Indian J. Pharm. Sci.* **2015**, *77*, 83.
(26) Gao, X.; Cao, Y.; Song, X.; Zhang, Z.; Zhuang, X.; He, C.; Chen, X. Biodegradable, p H-R esponsive Carboxymethyl Cellulose/P oly (Acrylic Acid) Hydrogels for Oral Insulin Delivery. *Macromol. Biosci.* **2014**, *14*, 565−575.
(27) Gahlawat, N.; Verma, R.; Kaushik, D. Application of D-optimal Mixture Design for Development and Optimization of Olmesartan Medoxomil Loaded SMEDDS. *Curr. Drug Ther.* **2020**, *15*, 548−560.
(28) Li, B.-L.; Zhang, J.; Jin, W.; Chen, X.-Y.; Yang, J.-M.; Chi, S.-M.; Ruan, Q.; Zhao, Y. Oral administration of pH-responsive polyamine modified cyclodextrin nanoparticles for controlled release of anti-tumor drugs. *React. Funct. Polym.* **2022**, *172*, No. 105175.
(29) Dudhipala, N.; Ay, A. A. Amelioration of ketoconazole in lipid nanoparticles for enhanced antifungal activity and bioavailability through oral administration for management of fungal infections. *Chem. Phys. Lipids* **2020**, *232*, No. 104953.
(30) Maddiboyina, B.; Desu, P. K.; Vasam, M.; Challa, V. T.; Surendra, A. V.; Rao, R. S.; Alagarsamy, S.; Jhawat, V. An insight of nanogels as novel drug delivery system with potential hybrid nanogel applications. *J. Biomater. Sci., Polym. Ed.* **2021**, *33* (2), 262−278.
(31) Huang, L.; Chaurasiya, B.; Wu, D.; Wang, H.; Du, Y.; Tu, J.; Webster, T. J.; Sun, C. Versatile redox-sensitive pullulan nanoparticles for enhanced liver targeting and efficient cancer therapy. *Nanomed. Nanotechnol. Biol. Med.* **2018**, *14*, 1005−1017.
(32) Yadav, R. Fabrication and Characterization of Sol-Gel Based Nanoparticles for Drug Delivery, 2014.
(33) Dhua, M.; Sen, K. K.; Maiti, S. Carboxylated gums as additives in the production of interpenetrating hydrogel beads and slow release of glimepiride. *J. Vinyl Addit. Technol.* **2022**, *28*, 518−529.
(34) Farias-Aguilar, J. C.; Ramírez-Moreno, M. J.; Téllez-Jurado, L.; Balmori-Ramírez, H. Low pressure and low temperature synthesis of polyamide-6 (PA6) using Na0 as catalyst. *Mater. Lett.* **2014**, *136*, 388−392.
(35) Ijaz, H.; Tulain, U. R.; Qureshi, J. Formulation and in vitro evaluation of pH-sensitive crosslinked xanthan gum-grafted acrylic acid copolymer for controlled delivery of perindopril erbumine (PE). *Polym.-Plast. Technol. Eng.* **2018**, *57*, 459−470.
(36) Minhas, M. U.; Ahmad, M.; Ali, L.; Sohail, M. Synthesis of chemically crosslinked polyvinyl alcohol-co-poly (methacrylic acid) hydrogels by copolymerization; a potential graft-polymeric carrier for oral delivery of 5-fluorouracil. *DARU J. Pharm. Sci.* **2013**, *21*, No. 44.
(37) Mahmood, A.; Mahmood, A.; Sarfraz, R. M.; Hussain, Z.; Afzal, A.; Boublia, A.; Bhutto, J. K.; Alreshidi, M. A.; Yadav, K. K.; Elboughdiri, N.; Benguerba, Y. Chitosan-based intelligent polymeric networks for site-specific colon medication delivery: A comprehensive study on controlled release of diloxanide furoate and network formation dynamics. *Int. J. Bio. Mac. Mole.* **2024**, *255*, 128089.
(38) Ijaz, H.; Tulain, U. R. Development of interpenetrating polymeric network for controlled drug delivery and its evaluation. *Int. J. Polym. Mater. Polym. Biomater.* **2019**, *68*, 1099−1107.
(39) Bajpai, S. K.; Singh, S. Analysis of swelling behavior of poly (methacrylamide-co-methacrylic acid) hydrogels and effect of synthesis conditions on water uptake. *React. Funct. Polym.* **2006**, *66*, 431−440.

https://doi.org/10.1021/acsomega.3c08107
ACS Omega 2024, 9, 10498−10516

(40) Wen, P.; Wu, Z.; He, Y.; Ye, B. C.; Han, Y.; Wang, J.; Guan, X. Microwave-assisted synthesis of a semi-interpenetrating polymer network slow-release nitrogen fertilizer with water absorbency from cotton stalks. *ACS Sustainable Chem. Eng.* **2016**, *4*, 6572−6579.
(41) Ijaz, H.; Tulain, U. R.; Minhas, M. U.; Mahmood, A.; Sarfraz, R. M.; Erum, A.; Danish, Z. Design and in vitro evaluation of pH-sensitive crosslinked chitosan-grafted acrylic acid copolymer (CS-co-AA) for targeted drug delivery. *Int. J. Polym. Mater. Polym. Biomater.* **2022**, *71*, 336−348.
(42) Liu, T. Y.; Chen, S. Y.; Lin, Y. L.; Liu, D. M. Synthesis and characterization of amphiphatic carboxymethyl-hexanoyl chitosan hydrogel: water-retention ability and drug encapsulation. *Langmuir* **2006**, *22*, 9740−9745.
(43) Biswal, S.; Sahoo, J.; Murthy, P. N.; Giradkar, R. P.; Avari, J. G. Enhancement of dissolution rate of gliclazide using solid dispersions with polyethylene glycol 6000. *AAPS PharmSciTech* **2008**, *9*, 563−570.
(44) Ijaz, H.; Tulain, U. R.; Azam, F.; Qureshi, J. Thiolation of arabinoxylan and its application in the fabrication of pH-sensitive thiolated arabinoxylan grafted acrylic acid copolymer. *Drug Dev. Ind. Pharm.* **2019**, *45*, 754−766.
(45) Anwar, H.; Ahmad, M.; Minhas, M. U.; Rehmani, S. Alginate-polyvinyl alcohol based interpenetrating polymer network for prolonged drug therapy, optimization and in-vitro characterization. *Carbohydr. Polym.* **2017**, *166*, 183−194.
(46) Parikh, R.; Patel, L.; Dalwadi, S. Microparticles of rifampicin: comparison of pulmonary route with oral route for drug uptake by alveolar macrophages, phagocytosis activity and toxicity study in albino rats. *Drug Delivery* **2014**, *21*, 406−411.
(47) Pandav, S.; Naik, J. Preparation and in vitro evaluation of ethylcellulose and polymethacrylate resins loaded microparticles containing hydrophilic drug. *J. Pharmaceutics* **2014**, *2014*, No. 904036, DOI: 10.1155/2014/904036.
(48) Mahmood, A.; Mahmood, A.; Sarfraz, R. M.; Ijaz, H.; Zafar, N.; Ashraf, M. U. Hydrogel-based intelligent delivery system for controlled release of diloxanide furoate. *Polym. Bull.* **2023**, *80*, 8283−8319.
(49) Jayaramudu, T.; Raghavendra, G. M.; Varaprasad, K.; Reddy, G. V. S.; Reddy, A. B.; Sudhakar, K.; Sadiku, E. R. Preparation and characterization of poly(ethylene glycol) stabilized nano silver particles by a mechanochemical assisted ball mill process. *J. Appl. Polym. Sci.* **2016**, *133* (7), 43027.
(50) Abdelquader, M. M.; Essa, E. A.; El Maghraby, G. M. Inhibition of co-crystallization of olmesartan medoxomil and hydrochlorothiazide for enhanced dissolution rate in their fixed dose combination. *AAPS PharmSciTech* **2019**, *20*, No. 3.
(51) Datt, N.; Yadav, P.; Poonuru, R. R. Development and Characterization of Microwave Irradiated Solid Dispersion Lipid Nanoparticles Containing Topical Gel for Dermatophytosis. *J. Pharm. Negative Results* **2022**, *13* (09), 2508−2516.
(52) Wang, L.; Li, S.; Tang, P.; Yan, J.; Xu, K.; Li, H. Characterization and evaluation of synthetic 624 riluzole with β-cyclodextrin and 2, 6-di-O-methyl-β-cyclodextrin inclusion complexes, 625 Carbohydrate. *Polymer* **2015**, *129*, 9−16.
(53) Gong, C. Y.; Dong, P. W.; Shi, S.; Fu, S. Z.; Yang, J. L.; Guo, G.; Qian, Z. Y. Thermosensitive PEG−PCL−PEG hydrogel controlled drug delivery system: sol−gel−sol transition and in vitro drug release study. *J. Pharm. Sci.* **2009**, *98*, 3707−3717.
(54) Moradkhannejhad, L.; Abdouss, M.; Nikfarjam, N.; Shahriari, M. H.; Heidary, V. The effect of molecular weight and content of PEG on in vitro drug release of electrospun curcumin loaded PLA/PEG nanofibers. *J. Drug Delivery Sci. Technol.* **2020**, *56*, No. 101554.
(55) Silk, J. C. Development of a globally harmonized system for hazard communication. *Int. J. Hyg. Environ. Health* **2003**, *206*, 447−452.

https://doi.org/10.1021/acsomega.3c08107
ACS Omega 2024, 9, 10498−10516